The primary function of gp130 signaling in osteoblasts is to maintain bone formation and strength, rather than promote osteoclast formation

Rachelle W Johnson[1], Holly J Brennan[1,2], Christina Vrahnas[1], Ingrid J Poulton[1], Narelle E McGregor[1], Therese Standal[1,3], Emma C Walker[1], Thuan-Tzen Koh[1], Huynh Nguyen[4], Nicole C Walsh[1,2], Mark R. Forwood[4], T John Martin[1,2], Natalie A Sims[1,2]

[1]St. Vincent's Institute of Medical Research, Fitzroy, Victoria, Australia

[2]University of Melbourne, Department of Medicine at St. Vincent's Hospital, Fitzroy, Victoria, Australia

[3]Department of Cancer Research and Molecular Medicine, Norwegian University of Science and Technology, Trondheim, Norway

[4]School of Medical Science, Griffith University, Gold Coast, Queensland, Australia

Corresponding author:

Natalie A Sims

9 Princes St

Fitzroy, Victoria 3122

Australia

Email: nsims@svi.edu.au

Phone: +613-9288-2555

Fax: +613-9416-2676

Running title: Osteocytic gp130 signalling

Supplemental data: 6 figures

Abstract

Interleukin-6 (IL-6) family cytokines act via gp130 in the osteoblast lineage to stimulate formation of osteoclasts (bone resorbing cells), activity of osteoblasts (bone forming cells) and to inhibit expression of the osteocyte protein, sclerostin. We report here that a profound reduction in trabecular bone mass occurs both when gp130 is deleted in the entire osteoblast lineage (Osx1Cre gp130 f/f) and when this deletion is restricted to osteocytes (DMP1Cre gp130 f/f). This was caused not by an alteration in osteoclastogenesis, but with a low level of bone formation specific to the trabecular compartment. In contrast, at the periosteal surface of the diaphysis, bone formation increased cortical diameter to maintain ultimate bone strength, despite a weak cortical bone matrix and reduced collagen type 1 production. We conclude that osteocytic gp130 signalling is required for normal trabecular bone mass and healthy cortical bone composition, suggesting that stimulating gp130 signalling in osteocytes could increase bone mass and strength.

Introduction

Osteoporosis results from imbalanced bone remodelling in which the level of bone resorption, carried out by osteoclasts, exceeds that of bone formation, carried out by osteoblasts. This leads to reduced bone mass in both the trabecular and cortical bone compartments. Both osteoblast and osteoclast formation are stimulated by cytokines that signal through glycoprotein 130 (gp130), a signal transducer utilized by the many different interleukin-6 (IL-6) family cytokines, including IL-6, interleukin-11 (IL-11), leukemia inhibitory factor (LIF), oncostatin M (OSM), ciliary neurotrophic factor (CNTF), and cardiotrophin-1 (CT-1) (1). Cytokine-specific knockout mouse models have established unique and necessary roles for each of these cytokines in physiological regulation of longitudinal growth, periosteal expansion and trabecular structure (2-9), as well as bone loss associated with inflammation (10) and estrogen deficiency (11).

Although gp130 is ubiquitously expressed (1), stimulation of osteoclast formation by IL-6, IL-11, LIF, CT-1, and OSM depends on the presence of osteoblasts *in vitro* (12,13) and is mediated by increased osteoblast RANKL mRNA expression (12-15). Furthermore, stimulation of osteoclast formation by other agents such as IL-1, PTH and 1,25-dihydroxyvitamin D_3, are also mediated, at least in part, by gp130 (3). However, the role of osteoblast lineage gp130 signalling in osteoclast formation is not well defined, and has been complicated by conflicting effects on osteoclast formation by genetic deletion of individual cytokines that signal via gp130 and phenotypic differences between the sexes *in vivo* (1). For example, systemic deletion of OSMR (6) inhibited osteoclast formation in male and female mice. A similar phenotype was reported in male mice with systemic deletion of IL-11R (16), but females showed only a reduction in osteoblastogenesis. In contrast, CT-1 knockout mice (9) had increased formation of osteoclasts with impaired activity in both males and females.

Further complicating the data, systemic LIF (5), LIFR (17) or gp130 deletion (18) resulted in increased numbers of large, active osteoclasts clustered near the growth plate in neonate mice. The contrasting nature of these *in vivo* osteoclast phenotypes are remarkable, given the strong stimulatory effects of OSM, IL-6, CT-1 and IL-11 on osteoclast formation *in vitro* (13,19).

IL-6 family cytokines also act on the osteoblast lineage to stimulate bone formation. IL-6, IL-11, CT-1 and OSM all promote osteoblast differentiation *in vitro* (9,20), and OSM, CT-1, and LIF stimulate bone formation *in vivo* (6,9,21). OSM, CT-1, LIF and IL-11 also inhibit adipocyte differentiation (5,6,9), suggesting an influence of these cytokines on early osteoblast precursor commitment. Furthermore, OSM, CT-1, IL-11 and LIF influence terminally differentiated osteoblasts embedded within the bone matrix (osteocytes), by suppressing their production of sclerostin (6), a potent inhibitor of Wnt signalling and bone formation (22). This indicates that IL-6 family cytokines act on osteoblasts at all stages of differentiation (e.g. early osteoblasts, late osteoblasts, or osteocytes), but the relevant stages at which they support bone formation, bone resorption or adipogenesis are unknown (23).

To determine the stage-specific roles of gp130 in the osteoblast lineage in both bone modelling and remodelling, we have generated two mouse models where gp130 was conditionally deleted either from the entire osteoblast lineage (Osx1Cre) or specifically in osteocytes (DMP1Cre). The data reported here indicate that gp130 signalling in the commited osteoblast lineage is not required for osteoclast differentiation in trabecular bone. Rather, the key role of gp130 signalling in the osteoblast lineage is in osteocytes, where it maintains bone formation in trabecular bone and cortical bone strength.

Materials and Methods

Animals. All animal procedures were conducted with approval of the St. Vincent's Health Melbourne Animal Ethics Committee. Osx1Cre mice backcrossed to C57BL/6 were obtained from Carl Walkley (St. Vincent's Institute, Fitzroy, Australia) (24) and DMP1Cre mice (containing the *DMP1* 10-kb promoter region) were obtained from Lynda Bonewald (University of Kansas, Kansas City, USA) (25). Floxed gp130 mice backcrossed onto C57BL/6 mice were obtained from Rodger McEver (Oklahoma Medical Research Foundation) (26). Mice hemizygous for the Cre transgene of each strain were crossed with a gp130 flox mouse in which the transmembrane domain (exon 15) was flanked by loxP sites, resulting in ablation of intracellular gp130 signalling, as previously reported (27). For all experiments, appropriate Cre+ wildtype littermates or cousins were used as controls. Both male and female mice were analysed, as indicated below.

Samples for histomorphometry, microCT, RNA and serum analyses were collected at 6, 12 and 26 weeks of age, after injection with calcein at 3 and 10 days prior to tissue collection (28). 12 week-old *DMP1.gp130* and *Osx1Cre.gp130 w/w* and *f/f* mice (n=6/7 per genotype) were fasted for 12 hours prior to anesthesia with ketamine/xylazine and blood collection via cardiac puncture. Blood samples were centrifuged 10 minutes at 4,000 rpm and serum supernatant was removed to a fresh tube and stored at -80^{o}C until analysis for CTX-1 or P1NP (Immunodiagnostic Systems Limited, Boldon, Tyne & Wear, UK) as per manufacturer's instructions. Flushed femurs from 12-week old *DMP1Cre.gp130*$^{w/w}$ and *DMP1Cre.gp130*$^{f/f}$ mice were harvested for RNA extraction as previously described (29).

Fluorescence activated cell sorting (FACS). *Osx1Cre.gp130*$^{w/w}$ and *Osx1Cre.gp130*$^{f/f}$ neonates were euthanized by decapitation and calvaria were dissected out for digestion in 1:2 collagenaseII/dispase solution (1 x 5 minutes, 4 x 10 minute digestions) shaking at 37^{o}C.

Collagenase/dispase solution was removed and cells were re-suspended in appropriate volume of FACS buffer (1XPBS, 2% FBS, 0.5mM EDTA) and sorted on a FACS Aria (BD Biosciences, San Jose, California) for GFP fluorescence driven by Cre transgene expression. Sorted cells were harvested for RNA in Trizol (Life Technologies, Carlsbad, California) and separated and precipitated using chloroform and isopropanol. Extracted RNA was DNase treated using Ambion TURBO DNA-free kit (Life Technologies) and measured on a NanoDrop ND1000 spectrophotemeter (Thermo Scientific, Wilmington, DE).

Injections. Five consecutive injections of 0.2µg mOSM or saline in 25µl volume were performed over the calvariae at 24 hours intervals on 6-week old female *DMP1Cre.gp130*$^{w/w}$ and *DMP1Cre.gp130*$^{f/f}$ mice via subcutaneous injection as previously described (9). Calvaria were harvested upon sacrifice, 10 days after the last injection, and analysed by histomorphometry as previously described (9).

Histomorphometry and microCT. Histomorphometry was performed on tibial sections as previously described (30). *Ex vivo* microCT was performed on femoral, vertebral, and calvarial specimens using the SkyScan 1076 system (Bruker-microCT, Kontich, Belgium). Images were acquired using the following settings: 9µm voxel resoluation, 0.5mm aluminum filter, 50kV voltage and 100µA current, exposure time, rotation 0.5^{o}, frame averaging =1. Images were reconstructed and analysed using SkyScan software programs NRecon (version 1.6.3.3), DataViewer (version 1.4.4) and CT Analyser (version 1.12.0.0). Femoral trabecular analysis region of interest (ROI) was determined by identifying the distal end of the femur and calculating 15% of the total femur length towards the femora mid-shaft, where we then analysed an ROI of 12.6% of the total femur length. Analysis of bone structure was completed using adaptive thresholding (mean of min and max values) in CT Analyser.

Thresholds for analysis were determined manually based on grayscale values for each experimental group as follows: Trabecular bone 12-week old mice: *Osx1Cre.gp130,* 38-255; *DMP1Cre.gp130,* 42-255. Trabecular bone 26 week-old mice: *Osx1Cre.gp130* and *DMP1Cre.gp130,* 42-255. Cortical analyses were performed 35% above the distal end of the femur toward the femora mid-shaft, also with a 12.6% ROI with the threshold values set as follows: Cortical bone, 12 week-old mice: *Osx1Cre.gp130,* 63-255; *DMP1Cre.gp130,* 57-255. Cortical bone, 26 week-old mice: *Osx1Cre.gp130* and *DMP1Cre.gp130,* 100-255. Vertebral trabecular bone was evaluated in the L6 vertebral body of 12 week-old mice, where the ROI was defined as a cylinder measuring 50% of the total height and 66% of the width of the vertebral column at the midpoint. Thresholds were as follows: *Osx1Cre.gp130,* 42-255; *DMP1Cre.gp130,* 50-255. Polarized light microscopy was performed on 100μm thick transverse sections collected approximately 500μm from the tip of the distal femur using an Isomet Saw, and measurements included the entire bone interface.

Semi-quantitative real-time PCR (qPCR). cDNA synthesis from 0.1-1μg DNase-treated RNA was performed using AffinityScript (Agilent Technologies, Santa Clara, California, USA) per the manufacturer's instructions. Stock cDNA was diluted 1:5-1:10 and semi-quantitative real-time PCR was performed using in-house master mix of 10X AmpliTaq Gold with SYBR Green nucleic acid gel stain (Life Technologies). Primers were used as previously published (31) or designed using Primer Blast (NCBI) and are reported in Table 1. Samples were dispensed onto an optically clear 96-well plate (Thermo Scientific) and run on a Stratagene Mx3000P (Agilent Technologies). Cycling conditions are (95^{o}C for 10:00), (95^{o}C for :30, 58^{o}C for 1:00, 72^{o}C for :30) X 40 cycles, followed by dissociation step (95^{o}C for 1:00, 55^{o}C for :30, 95^{o}C for :30). Post-run samples were analysed using Stratagene software MxPro and reported using linear ΔCT values normalized to β-2 microglobulin

(β2M) or hypoxanthine phosphoribosyltransferase 1 (HPRT1) for primary mouse cells or hydroxymethylbilane synthase (HMBS) for femoral extracts.

Mechanical testing. Femora from 26 week-old male and female *DMP1Cre.gp130* mice (males n=8 *w/w*, n=8 *f/f*; females n=5 *w/w*, n=7 *f/f*) were tested at the mid-shaft by three-point bending at room temperature. Load was applied in the anteroposterior (AP) direction midway between two supports that were 6.0 mm apart. Load-displacement curves were recorded at a crosshead speed of 1.0 $mm.sec^{-1}$ using an Instron 5565A dual column materials testing system, using Bluehill 2 software (Instron, Norwood MA, USA). Prior to testing they were kept moist in gauze swabs soaked in phosphate buffered saline (PBS). Ultimate force (F_U; N), yield force (F_Y; N), stiffness (S; $N.mm^{-1}$), and energy (work) to failure (U; mJ) were calculated from the load-displacement curves as described previously (32). The yield point was determined from the load deformation curve at the point at which the curve deviated from linear. Widths of the cortical mid-shaft in the medio-lateral (ML) and AP directions were measured using digital calipers, and the average cortical thickness was determined by microCT. Combining the geometric calculations and the biomechanical test results, the material properties of each bone were calculated as described by Schrieffer et al (33) to obtain ultimate stress (σ, MPa); elastic modulus (E, MPa), and modulus of toughness (*u*, MPa). Average load-deformation and stress-strain curves for each sex and genotype were also generated.

Reference Point Indentation. Local bone material properties at the femur mid-shafts from 12 week-old male *DMP1Cre.gp130* mice (males n=5 *w/w*, n=9 *f/f*; females n=5 *w/w*, n=5 *f/f*) were examined by reference point indentation using a BP2 probe assembly apparatus (Biodent Hfc, Active Life Scientific Inc.). The BP2 assembly includes a 90^o cono-spherical

Test Probe with a ≤ 5μm radius point and flat bevel Reference Probe with ~5mm cannula length and friction < 0.1N. To assure consistency between measurements a line 6mm from the femoral condyles was marked with pencil to indicate the initial probe position. To achieve a maximum indentation force of 2N, a specific load of 300g (reference force) was manually applied onto the femur. Two Newtons of force were applied for 10 cycles. Samples were kept partially hydrated with 70% ethanol during measurements. Internal friction, defined as the force resisting motion between the test and reference probe, was identified by the size and shape of the force-distance graph and kept at a constant of ≤0.3N to ensure that disruptions within the probe assembly would not affect results. Test measurements were taken pre- and post-experiment on polymerized methyl methacrylate (MMA) to ensure that measurements were consistent and that there were no probe faults throughout the course of the study. Data was discarded if graphs displayed high friction, or disruptions in the curves of the loading and unloading slopes. The distance the probe travels into the bone (total indentation distance, TDI) is a measure of the bone's resistance to fractures, indentation distance increase (IDI) is the indentation distance in the last cycle relative to the first cycle, and is correlated to bone tissue roughness, average unloading slope indicates the compressibility of the bone and can be used as a measure of stiffness (34).

Statistics. All graphs are represented as the mean/genotype or the mean of n=3 *in vitro* biological replicates. N is reported for each graph, with a range of 5-23 animals/group as indicated on the graph or in the figure legend. For *in vitro* experiments, 3 biological replicates were performed and averaged. All error bars are standard error of the mean (SEM). Statistical significance was considered $p<0.05$. All statistics were calculated using unpaired Student's t-test or 1-way ANOVA (GraphPad software) or as indicated in the figure legends.

Results

Confirmation of deletion of functional gp130

Knockdown of gp130 was confirmed in FACS-sorted Osx1Cre-GFP-expressing neonate calvarial osteoblasts, which indicated a 70% reduction in gp130 expression in *Osx1Cre.gp130*$^{f/f}$ cells compared to controls (Fig. 1A). Since the DMP1Cre construct does not contain a reporter element, gp130 knockdown of approximately 50% was verified in RNA from whole femurs, flushed of marrow, from both male and female 12-week old mice (Fig. 1B).

To confirm deletion of functional response of gp130, *DMP1Cre.gp130*$^{f/f}$ female mice and their controls were injected with OSM over the calvaria to stimulate bone formation (6). While *DMP1Cre.gp130*$^{w/w}$ mice formed additional bone in response to OSM, *DMP1Cre.gp130*$^{f/f}$ mice did not (Fig. 1C). Furthermore, the increase in calvarial thickness and greater mineral apposition rate (MAR) in response to OSM in *DMP1Cre.gp130*$^{w/w}$ mice was completely ablated by osteocytic deletion of gp130 (Fig. 1C).

gp130 in the osteoblast lineage maintains trabecular bone volume

MicroCT analysis of trabecular bone structure revealed a significantly lower trabecular bone volume (BV/TV) and trabecular number (TbN) (Fig. 2A&C), and significantly greater trabecular spacing (TbSp) in the femur (Fig. 2D) and vertebrae (Fig. S1) of male *Osx1Cre.gp130*$^{f/f}$ mice compared to *Osx1Cre.gp130*$^{w/w}$ controls at 12 and 26 weeks of age. Histomorphometric analysis of the proximal tibia confirmed this phenotype (Fig. S2), and detected significantly lower trabecular thickness in *Osx1Cre.gp130*$^{f/f}$ 12 week-old mice (Fig. S2B). *Osx1Cre.gp130*$^{w/f}$ heterozygote mice demonstrated no significant alteration in

trabecular structure at 12 weeks of age (data not shown). 6 week-old *Osx1Cre.gp130$^{f/f}$* mice did not exhibit a skeletal phenotype (Fig. S2), suggesting gp130 signaling in the osteoblast lineage is not required for bone growth.

To determine the stage of osteoblast differentiation at which gp130 is most important for maintaining trabecular bone structure, we used an identical approach to assess trabecular bone structure in 12 and 26 week-old *DMP1Cre.gp130$^{f/f}$* males (Fig. 3). MicroCT evaluation of femoral (Fig. 3) and vertebral (Fig. S3) trabecular bone structure revealed a low BV/TV (Fig. 3A) and TbN (Fig. 3C) in *DMP1Cre.gp130$^{f/f}$* mice compared to *DMP1Cre.gp130$^{w/w}$* controls, and a significant increase in TbSp at both 12 and 26 weeks of age (Fig. 3D). This method also detected a modest, but significantly greater trabecular thickness in *DMP1Cre.gp130$^{f/f}$* mice compared to *DMP1Cre.gp130$^{w/w}$* at both 12 and 26 weeks (Fig. 3B). Histomorphometric assessment of the tibia confirmed the low BV/TV and TbN at both 12 and 26 weeks (Fig. S4). *DMP1Cre.gp130$^{w/f}$* heterozygous mice at 12 weeks of age demonstrated a significant increase in tibial TbTh (by 12.7%, $p<0.001$) and TbSp (by 34.5%, $p<0.01$) by microCT (data not shown).

Neonate *Osx1Cre.gp130$^{f/f}$* and *DMP1Cre.gp130$^{f/f}$* mice did not show any significant skeletal or morphological defects, indicating that gp130 in the osteoblast lineage is not required for normal bone development.

Conditional deletion of gp130 in osteocytes and osteoblasts inhibits trabecular bone formation, but not osteoclast formation

Dynamic histomorphometry revealed that the low bone mass of *DMP1Cre.gp130$^{f/f}$* and *Osx1Cre.gp130$^{f/f}$* mice was associated with a low rate of bone formation. Both *DMP1Cre.gp130$^{f/f}$* (Fig. 4A) and *Osx1Cre.gp130$^{f/f}$* (Fig. 4B) male mice demonstrated 30% lower trabecular bone formation rate (BFR) compared to their respective *w/w* controls. This was attributed to significantly lower mineralising surface (dLS/BS), not a low mineral apposition rate (MAR) (Fig. 4), suggesting impaired osteoblast differentiation in both strains of mice. However, no significant changes in osteoblast number (ObN/BPm), osteoblast surface/bone surface (ObS/BS), osteoid surface (OS/BS) or osteoid volume (OV/BV) were observed in male *DMP1Cre.gp130$^{f/f}$* or *Osx1Cre.gp130$^{f/f}$* mice (Table 2). This may relate to the already low baseline values of these parameters in 12 week-old male mice, making any further reduction difficult to detect.

In 12 week-old female mice, where osteoblast numbers and extent of osteoid are significantly greater than in male mice (35), we detected significantly lower NOb/BPm and ObS/BS (Table 2) as well as reduced BFR in *DMP1Cre.gp130$^{f/f}$* (Fig. 4C) and *Osx1Cre.gp130$^{f/f}$* (Fig. 4D) mice compared to controls, confirming reduced osteoblast differentiation in the absence of osteocyte gp130. To determine whether this was associated with diversion towards the adipocyte lineage, marrow adipocyte numbers were evaluated in *Osx1Cre.gp130$^{f/f}$* mice, and were at wildtype levels in both male and female 12 week-old mice (data not shown).

Despite the known influence of IL-6 family cytokines on osteoclastogenesis, osteoclast number (NOc/BPm), surface/bone surface (OcS/BS), and length (OcL) were not significantly different in *DMP1Cre.gp130$^{f/f}$* or *Osx1Cre.gp130$^{f/f}$* male or female mice compared to controls (Table 2).

Cortical circumference is increased with gp130 deletion in the osteoblast lineage

The cortical bone phenotypes of *DMP1Cre.gp130* 12 and 26 week-old male mice (Fig. 5A) were strikingly different to those observed in trabecular bone. Although there was no change in bone length (Fig. S5) or cortical thickness (data not shown), femoral periosteal perimeter (PsPm), mean cross-sectional moment of inertia (CSMI), and marrow area were all significantly greater in *DMP1Cre.gp130*$^{f/f}$ male mice (Fig. 5A) compared to controls. This reflected increased bone width in both the anterior-posterior and lateral-medial directions (Fig. 5B). A similar cortical phenotype was observed in female *DMP1Cre.gp130*$^{f/f}$ mice at 26 weeks of age (data not shown), in 12 week-old male *Osx1Cre.gp130*$^{f/f}$ mice (Fig. 5C) and in 12 and 26 week-old female *Osx1Cre.gp130*$^{f/f}$ mice (data not shown). At 26 weeks of age there was no difference in cortical bone mass between *Osx1Cre.gp130*$^{f/f}$ and *w/w* controls mice due to delayed bone accrual in the *w/w* group, an effect of the Osx1Cre transgene that has been previously noted (36).

In contrast to their low trabecular BFR, *DMP1Cre.gp130*$^{f/f}$ and *Osx1Cre.gp130*$^{f/f}$ mice formed periosteal bone at the same rate and along the same extent of surface as their respective *w/w* controls at 12 weeks (Fig. 5D&E) and at 6 and 26 weeks (data not shown); this was also found in transverse sections of femurs from 12 week-old *DMP1Cre.gp130* mice (data not shown). There was also no detectable difference in endocortical mineralising surface, mineral apposition rate, bone formation rate, osteoclast number, or osteoclast surface in 12 week-old mice (data not shown). This indicates that the larger cortical diameter is caused by a level of bone formation slightly greater than control throughout bone growth, but at a level too low to be detectably greater at any single time point (i.e. 6, 12 and 26 weeks).

gp130 in osteocytes maintains cortical material properties

Since CSMI and marrow area were significantly greater in the absence of gp130 in both *Osx1Cre.gp130$^{f/f}$* and *DMP1Cre.gp130$^{f/f}$* mice, mechanical properties of the femoral mid-shaft were evaluated in 26 week-old *DMP1Cre.gp130$^{w/w}$* and *DMP1Cre.gp130$^{f/f}$* mice by 3-point bending test. Elastic modulus (intrinsic stiffness), ultimate stress and yield strength (level of stress at which permanent damage is initiated in the bone) were all significantly lower in male *DMP1Cre.gp130$^{f/f}$* mice (Fig. 6A-C), and elastic modulus was significantly lower in female *DMP1Cre.gp130$^{f/f}$* mice (Fig. 6A). Toughness (amount of energy required to fracture the bone) was also slightly lower in the males, but this was not statistically significant (Fig. 6D). Parameters that are not corrected for the altered size and shape of the bone (stiffness, failure force, deformation at failure, and energy absorbed at failure) were not significantly different in *DMP1Cre.gp130$^{f/f}$* males or females compared to *w/w* controls (Table 3), indicating that the structural integrity of the whole bone remained intact due to the increased cortical dimensions. The load-deformation graphs confirm no difference in response to mechanical load in either the male or female mice prior to normalization for bone geometry (Fig. 6E&F). In contrast, the average stress-strain curves demonstrate that after normalization for bone geometry, the *DMP1Cre.gp130$^{f/f}$* male bones are more compliant and withstand less stress than their wildtype counterparts (Fig. 6G&H). Post-yield stress was also significantly reduced in male *DMP1Cre.gp130$^{f/f}$* mice only (Figure 6I). Since the bones from the *DMP1Cre.gp130$^{f/f}$* males had poorer material properties, tissue mineral density was assessed by microCT on bones from 12 week-old mice (Fig. S6A) but no difference between *w/w* and *f/f* mice was detected.

To determine whether the poor matrix material properties were due to differences in the proportion of woven *vs* lamellar bone in *DMP1Cre.gp130$^{f/f}$* mice, 100μm transverse sections of 12 week-old male femora were analysed by polarized light microscopy. *DMP1Cre.gp130$^{f/f}$* mice showed a significantly higher proportion of disorganized woven bone compared to lamellar bone matrix in the proximal femur (Fig. 6J).

When 12 week-old bones from these mice were analysed by reference point indentation (RPI), there was no difference in total indentation distance, average loading or unloading slopes, or indentation distance increase after loading (Fig. S6B), suggesting that the poor material properties of *DMP1Cre.gp130$^{f/f}$* bones do not relate to a defect at the micro-indentation level.

Osteocyte density is greater in the trabecular compartment of gp130 osteocyte conditional knockout mice, resulting in greater local production of sclerostin

The trabecular compartment-specific reduction in bone formation rate in the absence of gp130 in osteocytes suggests that osteoblasts in the trabecular bone and periosteum respond differently to gp130 signals controlling bone formation. Since OSM, LIF, IL-11, and CT-1 all inhibit osteocyte production of the bone formation inhibitor sclerostin (6), the density of total osteocytes and sclerostin-positive osteocytes was assessed in 12 week-old male *Osx1Cre.gp130* and *DMP1Cre.gp130* cortical and trabecular bone to determine whether region-specific changes in osteocyte number and sclerostin production could explain the region-specific phenotype. Osteocyte density was no different in the trabecular *vs* cortical bone of the *Osx1Cre.gp130$^{f/f}$* mice (Fig. 7A). However, *Osx1Cre.gp130$^{f/f}$* mice had significantly more sclerostin-positive osteocytes in both trabecular and cortical bone than their *w/w* controls (Fig. 7B), suggesting that gp130 deletion early in the osteoblast lineage

increases the number of osteocytes that express sclerostin throughout trabecular and cortical bone.

In contrast to the *Osx1Cre.gp130$^{f/f}$* mice, there was no significant difference in total osteocyte density in trabecular bone between *DMP1Cre.gp130$^{w/w}$* and *DMP1Cre.gp130$^{f/f}$* mice. However, within *DMP1Cre.gp130$^{f/f}$* mice, there was a substantially greater numerical density of osteocytes in the trabecular bone compared to the cortical bone of the same mice (Fig. 7A). Again, this was in contrast to the *Osx1Cre.gp130$^{f/f}$* mice. Although the percent of sclerostin-positive osteocytes was not different between *DMP1Cre.gp130$^{w/w}$ and DMP1Cre.gp130$^{f/f}$* mice in the trabecular or cortical bone (data not shown), the greater total osteocyte density in trabecular bone compared to cortical bone resulted in significantly more sclerostin-positive osteocytes in trabecular bone compared to cortical bone in *DMP1Cre.gp130$^{f/f}$* mice (Fig. 7B), a difference that was not observed in control mice. Thus, the increased number of sclerostin-positive osteocytes is due only to an increase in the total number of osteocytes, not an increase in the proportion of sclerostin-producing osteocytes, and suggests other mechanisms are responsible for the differences in bone volume between *DMP1Cre.gp130$^{w/w}$* and *DMP1Cre.gp130$^{f/f}$* mice.

Since osteocyte sclerostin production was increased in both the trabecular and cortical bone, but only in *Osx1Cre.gp130$^{f/f}$* mice, these data also indicate that region-specific patterns of sclerostin production are not responsible for the region-specific phenotype observed in both *Osx1Cre.gp130$^{f/f}$* and *DMP1Cre.gp130$^{f/f}$* mice.

Osteocyte deletion of gp130 reduces osterix, collagen type 1-α1, and osteocalcin gene expression

To assess the effects of gp130 deletion on gene expression in bone, we determined differences in osteoblast and osteocyte marker genes in flushed femurs of *DMP1Cre.gp130*$^{f/f}$ mice with verified gp130 knockdown (Fig. 1B). mRNA levels of the early osteoblast marker osterix (Fig. 8A) and mature osteoblast marker osteocalcin (Fig. 8B), as well as collagen type 1-α1 (Fig. 8C), were all significantly lower (~50%) in bones from *DMP1Cre.gp130*$^{f/f}$ mice compared to *DMP1Cre.gp130*$^{w/w}$ mice. Notably, collagen type 1-α2 mRNA levels were not significantly changed in *f/f* bones (Fig. 8D). Thus the ratio of collagen type 1-α1: collagen type 1-α2, which normally exists in a 2:1 ratio, was reduced (Fig. 8E). Neither receptor activator of $NF_{\kappa}B$ ligand (RANKL; *Tnfsf11*) nor *Sost* mRNA levels were significantly different in *DMP1Cre.gp130*$^{f/f}$ mice compared to controls (Fig. 8F).

Discussion

This work demonstrates that the key cell through which gp130 controls trabecular bone formation and cortical bone strength is the osteocyte. Genetic deletion of gp130 in osteocytes results in very low trabecular bone formation rate and mass, and larger cortical bone diameter that compensates for significantly degraded cortical bone material properties and low collagen production. This regionally divergent phenotype was confirmed in a second model where gp130 was deleted in the entire osteoblast lineage. In neither model of gp130 deficiency was osteoclastogenesis altered. This leads us to conclude that the increased RANKL production in the osteoblast lineage that occurs in response to IL-6 family cytokines does not play a key role in physiological bone growth and remodeling, but it is the regulation of osteoblast differentiation and matrix production through the osteocyte that is the key role of gp130 in the osteoblast lineage (Fig. 9).

The findings of a low level of trabecular bone formation and increased cortical dimensions elicited by gp130 deletion in osteocytes is unique. It contrasts with osteocyte-specific knockouts of other pathways that stimulate bone formation (β-catenin, Pkd1 and IGF-1) which result in low bone mass in both cortical and trabecular bone due to reduced bone formation at both sites (37-39). These data suggest that stimulating gp130 signaling in osteocytes may increase trabecular bone formation and trabecular bone mass, without increasing osteoclast formation, a phenomenon that could be exploited therapeutically.

All IL-6 family members, apart from those that signal through CNTF receptor (CNTFR), stimulate osteoclast differentiation (1). This influence has been understood for many years to depend on the ability of these cytokines to stimulate RANKL production by osteoblast-lineage cells (12-15). This is supported by *in vitro* co-culture studies, where osteoclast formation in response to IL-6 family cytokines depended on the presence of osteoblasts (13,19), and osteoclast formation in response to other cytokines and hormones such as IL-1, PTH and 1,25-dihydroxyvitamin-D_3 was partially dependent on gp130 signalling (3). It was surprising, then, that we observed no change in osteoclast differentiation or RANKL expression when gp130 was deleted in the osteoblast lineage, or in osteocytes alone. In previous work, adult mice with global deletion of either OSMR or IL-11R demonstrated low levels of osteoclast formation (6,16), while increased numbers of osteoclasts with impaired activity were observed in mice lacking CT-1 (9). OSMR null osteoblasts were less supportive of osteoclast formation when stimulated with 1,25-dihydroxyvitamin-D_3 (6), but supported enhanced osteoclastogenesis in response to PTH (29), suggesting stimulus-dependent roles of osteoblastic gp130 signalling in support of osteoclastogenesis. In the cases of IL-11R and CT-1 deletion, altered osteoclast formation levels were intrinsic to the hemopoietic lineage (9,16). Importantly, in all of these mouse knockout models, the IL-6 family cytokine was

deleted systemically, and therefore it is unclear whether the effects on osteoclastogenesis in these mice was due to the absence of gp130 signalling in the osteoblast lineage. The data presented here indicate that osteoclast formation in physiological bone remodelling does not require gp130 signalling in the committed osteoblast lineage (Fig. 9A), and this is the first instance in which the absence of gp130 signalling was restricted to the osteoblast lineage. This supports the concept that RANKL expression induced by IL-6 family cytokinesin the osteoblast lineage may be most important in specific conditions of elevated osteoclast formation such as estrogen deficiency (11) or inflammatory arthritis (10). In addition, during bone development and growth, control of osteoclast formation by the IL-6 family may be restricted to the growth plate, as observed in the neonate-lethal LIFR and gp130 null mice (17,18) and adult LIF deficient mice (5). In this region, gp130-dependent osteoclastogenesis may be more directly controlled by hypertrophic chondrocytes than by the osteoblast lineage (5). This is further supported by a lack of bone phenotype in neonate or 6 week-old *Osx1Cre.gp130*$^{f/f}$ mice, indicating that gp130 signaling in the osteoblast lineage is not required for normal bone development, but its key role is to maintain bone formation in the physiological process of bone remodelling in the adult skeleton.

The low level of trabecular bone formation, lower osteoblast number, and reduced osterix, type 1 collagen and osteocalcin mRNA levels in *DMP1Cre.gp130*$^{f/f}$ bones confirms a critical role for osteocyte gp130 in promoting osteoblast differentiation (Fig. 9B). This confirms a physiological role for gp130 cytokines that stimulate bone formation *in vivo* and modify osteocyte gp130 signalling, such as OSM, CT-1, and LIF (6,9,40). This is further supported by the complete absence of an anabolic response to supra-calvarial injections of OSM in *DMP1Cre.gp130*$^{f/f}$ mice. This is also consistent with the known stimulatory effects of IL-6 family cytokines on bone formation (6,41), and low levels of trabecular bone formation

previously reported in mice with global deletion of LIF, CT-1, OSMR, IL-11R (5,6,9,16). Although IL-6 family members that stimulate bone formation also inhibit adipogenesis *in vitro* (5,6,9,16), no change in marrow adipogenesis was observed in the osteoblast or osteocyte specific knockouts (data not shown). This indicates that the anti-adipogenic action of IL-6 family cytokines is mediated by gp130 signalling in non-committed osteoblast precursors prior to osterix expression (Fig. 9A).

Deletion of gp130 in osteocytes led to decreased intrinsic bone strength (i.e. ultimate stress) in *DMP1Cre.gp130*$^{f/f}$ mice and increased the diaphyseal dimensions such that ultimate bending load remained unchanged. This means that the fracture resistance of the bones was retained despite a significant reduction in their material properties. This mechanical maintenance was achieved by an increase in periosteal dimensions, hence increased moment of inertia, to compensate for the decline in bone material quality. The modest increase in trabecular thickness, detected only by microCT, may also reflect this compensatory mechanism. Alternatively, since this slight increase in trabecular thickness was specific for the DMP1Cre model, which suggests that gp130 signaling in the osteocyte may limit the thickness of new trabeculae formed at the growth plate, and this limiting effect is negated when gp130 signaling is deleted throughout the osteoblast lineage. Accordingly, the low trabecular BFR reported here and measured in the secondary spongiosa reflects a lower rate of bone remodeling, not trabecular formation at the growth plate. Furthermore, the reduced material properties of the cortical bone in osteocytic gp130 deficiency suggests that gp130 signalling in osteocytes may improve collagen deposition during the osteoid production phase, or mineral deposition during matrix maturation (Fig. 9B,C). Since no significant alterations in tissue mineral density or periosteal MAR were detected in 12 week-old *DMP1Cre.gp130*$^{f/f}$ mice, the poor material properties of the bone matrix likely reflect a defect in collagen

deposition rather than altered mineralization. Indeed this was supported by our findings that the ratio of collagen 1 type α1 to type α2 mRNA levels was altered, and there was a higher proportion of woven bone in cortical samples of these mice. However, we cannot rule out an alteration in the distribution of mineral in the bones of *DMP1Cre.gp130$^{f/f}$* mice, particularly given the lower osteocalcin mRNA levels.

Although the *DMP1Cre.gp130$^{f/f}$* female bones were less stiff than their wildtype littermates, only male *DMP1Cre.gp130$^{f/f}$* bones had lower ultimate stress, yield strength, and post-yield stress. Previous work has demonstrated that slender bones have a higher degree of mineralization and tissue mineral density to compensate for their smaller bone size (42), as we have observed in the smaller diameter and higher tissue mineral density of the female *DMP1Cre.gp130$^{f/f}$* and control bones compared to males. The higher mineral content in the female bones may therefore provide some protection against the effect of gp130 deletion on bone stiffness.

Increased periosteal circumference has not been observed in any global gp130 knockout mouse models. In fact, IL-6, IL-11R, CT-1, and OSMR knockout models each show reduced periosteal circumference (2,3,6,9). This suggests that maintenance of cortical bone strength by increased periosteal apposition depends on influences of IL-6 family cytokines on other cell types that stimulate increased activity of periosteal osteoblasts. The increased periosteal expansion in *DMP1Cre.gp130$^{f/f}$* mice is likely to be a response to altered mechanical loading resulting from the poor material integrity. We were unable to detect an increase in periosteal bone formation on transverse and coronal sections at any single time point, which suggests that the periosteal expansion in these bones occurred slowly and over a long period of time, which may be indicative of a cumulative mechanical response over the life of the mouse.

This may also indicate that, even though OSM, OSMR and IL-11 mRNA levels in bone are increased in response to mechanical load (43), periosteal bone formation that is likely induced by mechanical forces may not require gp130 signalling in osteocytes (Fig. 9D).

More sclerostin-positive osteocytes were observed in both trabecular and cortical bone of *Osx1Cre.gp130*$^{f/f}$ mice compared to controls, but not in *DMP1Cre.gp130*$^{f/f}$ mice. This suggests that the inhibitory paracrine action of endogenous gp130 cytokines on sclerostin expression, previously described by pharmacological studies *in vivo* and *in vitro* (6) is mediated indirectly by an action on early osteoblasts. This increase in sclerostin-positive osteocytes was only observed in *Osx1Cre.gp130*$^{f/f}$ mice, suggesting it may contribute to the normal trabecular thickness in these mice, a phenotype that was not observed in the *DMP1Cre.gp130*$^{f/f}$ mice. Since both *Osx1Cre.gp130*$^{f/f}$ and *DMP1Cre.gp130*$^{f/f}$ mice exhibited low trabecular bone formation and large periosteal circumference, regulation of sclerostin production can be excluded as the primary driving force behind the change in bone structure observed in these mice.

The greater osteocyte density and low bone formation rate found specifically within the trabecular bone of the *DMP1Cre.gp130*$^{f/f}$ mice is consistent with reports in human bone, where trabecular osteocyte density and bone formation rate were negatively correlated (44). This suggests that IL-6 family cytokines, in addition to reducing sclerostin (6), may also determine the rate at which osteocytes become incorporated within the trabecular network. It is also possible that in the absence of osteocytic gp130 osteoblast apoptosis is impaired, and more osteoblasts survive through to osteocyte differentiation, consistent with previous in vitro reports of an anti-apoptotic role of IL-6 family cytokines (45). However, it remains

unclear why this was observed only in *DMP1Cre.gp130*$^{f/f}$ bones when the *Osx1Cre.gp130*$^{f/f}$ mice also exhibited low trabecular bone mass.

Therapeutic use of IL-6 inhibition for inflammation is widespread (46), and new IL-6 family inhibitors are actively being pursued for a wide range of disorders (47). Clinical trials have begun to test the efficacy of a soluble form of gp130 (sgp130-Fc) that selectively blocks IL-6 *trans*-signalling by sequestering the IL-6:sIL-6R complex and preventing it from binding membrane-bound IL-6R (48,49). These pathologic conditions already exhibit increased fracture risk, and our findings of detrimental effects of osteocyte gp130 inhibition on trabecular bone mass and cortical bone material properties, indicates careful skeletal monitoring of patients enrolled in future clinical trials is warranted.

In conclusion, we report here an essential role for osteocyte gp130 signalling to support trabecular bone formation and healthy composition of the cortical bone matrix. These data also suggest that stimulation of gp130 signalling targeted to the osteocyte may provide therapeutic benefit by stimulating trabecular bone formation and preserving material properties in the cortical bone.

Disclosures

The authors have no conflict of interest to disclose.

Acknowledgements

The authors thank Joshua Johnson for technical expertise in the processing of bone samples for histomorphometric analysis. The Victorian State Government Operational Infrastructure Support Scheme provides support to St. Vincent's Institute of Medical Research. This work was completed with financial support from the National Health and Medical Research Council of Australia. Authors' roles: Study design: NAS, RWJ. Study conduct: RWJ, HJB, CV, IJP, NEM, TS, ECW, TTK, HN. Data collection: RWJ, HJB, CV, IJP, NEM, TS, ECW, TTK, HN, NAS. Data analysis: RWJ, HJB, CV, IJP, HN, NCW, MRF and NAS. Data interpretation: RWJ, HJB, CV, NCW, MRF, TJM and NAS. Drafting manuscript: RWJ and NAS. Revising manuscript content: RWJ, TS, NCW, MRF, TJM and NAS. Approving final version of manuscript: RWJ, HJB, CV, IJP, NEM, TS, ECW, TTK, HN, NCW, MRF, TJM and NAS. NAS takes responsibility for the integrity of the data analysis.

References

1. Sims NA, Walsh NC 2010 GP130 cytokines and bone remodelling in health and disease. BMB Rep **43**(8)**:**513-523.
2. Ishimi Y, Miyaura C, Jin CH, Akatsu T, Abe E, Nakamura Y, Yamaguchi A, Yoshiki S, Matsuda T, Hirano T, Kishimoto T, Suda T 1990 IL-6 is produced by osteoblasts and induces bone resorption. Journal of immunology **145**(10)**:**3297-3303.
3. Romas E, Udagawa N, Zhou H, Tamura T, Saito M, Taga T, Hilton DJ, Suda T, Ng KW, Martin TJ 1996 The role of gp130-mediated signals in osteoclast development: regulation of interleukin 11 production by osteoblasts and distribution of its receptor in bone marrow cultures. J Exp Med **183**(6)**:**2581-2591.
4. Ishimi Y, Abe E, Jin CH, Miyaura C, Hong MH, Oshida M, Kurosawa H, Yamaguchi Y, Tomida M, Hozumi M, Suda T 1992 Leukemia inhibitory factor/differentiation-stimulating factor (LIF/D-factor): regulation of its production and possible roles in bone metabolism. J Cell Physiol **152**(1)**:**71-78.
5. Poulton IJ, McGregor NE, Pompolo S, Walker EC, Sims NA 2012 Contrasting roles of LIF in murine bone development and remodeling involve region-specific changes in vascularization. J Bone Miner Res **27**(4)**:**902-912.
6. Walker EC, McGregor NE, Poulton IJ, Solano M, Pompolo S, Fernandes TJ, Constable MJ, Nicholson GC, Zhang JG, Nicola NA, Gillespie MT, Martin TJ, Sims NA 2010 Oncostatin M promotes bone formation independently of resorption when signaling through leukemia inhibitory factor receptor in mice. J Clin Invest **120**(2)**:**582-592.
7. McGregor NE, Poulton IJ, Walker EC, Pompolo S, Quinn JM, Martin TJ, Sims NA 2010 Ciliary neurotrophic factor inhibits bone formation and plays a sex-specific role in bone growth and remodeling. Calcif Tissue Int **86**(3)**:**261-270.
8. Liu F, Aubin JE, Malaval L 2002 Expression of leukemia inhibitory factor (LIF)/interleukin-6 family cytokines and receptors during in vitro osteogenesis: differential regulation by dexamethasone and LIF. Bone **31**(1)**:**212-219.
9. Walker EC, McGregor NE, Poulton IJ, Pompolo S, Allan EH, Quinn JM, Gillespie MT, Martin TJ, Sims NA 2008 Cardiotrophin-1 is an osteoclast-derived stimulus of bone formation required for normal bone remodeling. J Bone Miner Res **23**(12)**:**2025-2032.
10. Wong PK, Quinn JM, Sims NA, van Nieuwenhuijze A, Campbell IK, Wicks IP 2006 Interleukin-6 modulates production of T lymphocyte-derived cytokines in antigen-induced arthritis and drives inflammation-induced osteoclastogenesis. Arthritis Rheum **54**(1)**:**158-168.
11. Poli V, Balena R, Fattori E, Markatos A, Yamamoto M, Tanaka H, Ciliberto G, Rodan GA, Costantini F 1994 Interleukin-6 deficient mice are protected from bone loss caused by estrogen depletion. The EMBO journal **13**(5)**:**1189-1196.
12. Tamura T, Udagawa N, Takahashi N, Miyaura C, Tanaka S, Yamada Y, Koishihara Y, Ohsugi Y, Kumaki K, Taga T, et al. 1993 Soluble interleukin-6 receptor triggers osteoclast formation by interleukin 6. Proc Natl Acad Sci U S A **90**(24)**:**11924-11928.
13. Richards CD, Langdon C, Deschamps P, Pennica D, Shaughnessy SG 2000 Stimulation of osteoclast differentiation in vitro by mouse oncostatin M, leukaemia

inhibitory factor, cardiotrophin-1 and interleukin 6: synergy with dexamethasone. Cytokine **12**(6)**:**613-621.
14. Palmqvist P, Persson E, Conaway HH, Lerner UH 2002 IL-6, leukemia inhibitory factor, and oncostatin M stimulate bone resorption and regulate the expression of receptor activator of NF-kappa B ligand, osteoprotegerin, and receptor activator of NF-kappa B in mouse calvariae. Journal of immunology **169**(6)**:**3353-3362.
15. Horwood NJ, Elliott J, Martin TJ, Gillespie MT 1998 Osteotropic agents regulate the expression of osteoclast differentiation factor and osteoprotegerin in osteoblastic stromal cells. Endocrinology **139**(11)**:**4743-4746.
16. Sims NA, Jenkins BJ, Nakamura A, Quinn JM, Li R, Gillespie MT, Ernst M, Robb L, Martin TJ 2005 Interleukin-11 receptor signaling is required for normal bone remodeling. J Bone Miner Res **20**(7)**:**1093-1102.
17. Ware CB, Horowitz MC, Renshaw BR, Hunt JS, Liggitt D, Koblar SA, Gliniak BC, McKenna HJ, Papayannopoulou T, Thoma B, Cheng L, Donovan PJ, Peschon JJ, Bartlett PF, Willis CR, Wright BD, Carpenter MK, Davison BL, Gearing DP 1995 Targeted disruption of the low-affinity leukemia inhibitory factor receptor gene causes placental, skeletal, neural and metabolic defects and results in perinatal death. Development **121**(5)**:**1283-1299.
18. Shin HI, Divieti P, Sims NA, Kobayashi T, Miao D, Karaplis AC, Baron R, Bringhurst R, Kronenberg HM 2004 Gp130-mediated signaling is necessary for normal osteoblastic function in vivo and in vitro. Endocrinology **145**(3)**:**1376-1385.
19. Tamura T, Udagawa N, Takahashi N, Miyaura C, Tanaka S, Yamada Y, Koishihara Y, Ohsugi Y, Kumaki K, Taga T, Kishimoto T, Suda T 1993 Soluble interleukin-6 receptor triggers osteoclast formation by interleukin 6. Proc Natl Acad Sci U S A **90**(24)**:**11924-11928.
20. Bellido T, Borba VZ, Roberson P, Manolagas SC 1997 Activation of the Janus kinase/STAT (signal transducer and activator of transcription) signal transduction pathway by interleukin-6-type cytokines promotes osteoblast differentiation. Endocrinology **138**(9)**:**3666-3676.
21. Metcalf D, Gearing DP 1989 Fatal syndrome in mice engrafted with cells producing high levels of the leukemia inhibitory factor. Proc Natl Acad Sci U S A **86**(15)**:**5948-5952.
22. Li X, Zhang Y, Kang H, Liu W, Liu P, Zhang J, Harris SE, Wu D 2005 Sclerostin binds to LRP5/6 and antagonizes canonical Wnt signaling. J Biol Chem **280**(20)**:**19883-19887.
23. Tonna S, Sims NA 2013 Talking among Ourselves: Paracrine Control of Bone Formation within the Osteoblast Lineage. Calcif Tissue Int.
24. Rodda SJ, McMahon AP 2006 Distinct roles for Hedgehog and canonical Wnt signaling in specification, differentiation and maintenance of osteoblast progenitors. Development **133**(16)**:**3231-3244.
25. Lu Y, Xie Y, Zhang S, Dusevich V, Bonewald LF, Feng JQ 2007 DMP1-targeted Cre expression in odontoblasts and osteocytes. J Dent Res **86**(4)**:**320-325.
26. Betz UA, Bloch W, van den Broek M, Yoshida K, Taga T, Kishimoto T, Addicks K, Rajewsky K, Muller W 1998 Postnatally induced inactivation of gp130 in mice results in neurological, cardiac, hematopoietic, immunological, hepatic, and pulmonary defects. J Exp Med **188**(10)**:**1955-1965.
27. Streetz KL, Wustefeld T, Klein C, Kallen KJ, Tronche F, Betz UA, Schutz G, Manns MP, Muller W, Trautwein C 2003 Lack of gp130 expression in hepatocytes promotes liver injury. Gastroenterology **125**(2)**:**532-543.

28. Sims NA, Clement-Lacroix P, Da Ponte F, Bouali Y, Binart N, Moriggl R, Goffin V, Coschigano K, Gaillard-Kelly M, Kopchick J, Baron R, Kelly PA 2000 Bone homeostasis in growth hormone receptor-null mice is restored by IGF-I but independent of Stat5. J Clin Invest **106**(9)**:**1095-1103.
29. Walker EC, Poulton IJ, McGregor NE, Ho PW, Allan EH, Quach JM, Martin TJ, Sims NA 2012 Sustained RANKL response to parathyroid hormone in oncostatin M receptor-deficient osteoblasts converts anabolic treatment to a catabolic effect in vivo. J Bone Miner Res **27**(4)**:**902-912.
30. Sims NA, Brennan K, Spaliviero J, Handelsman DJ, Seibel MJ 2006 Perinatal testosterone surge is required for normal adult bone size but not for normal bone remodeling. Am J Physiol Endocrinol Metab **290**(3)**:**E456-462.
31. Allan EH, Hausler KD, Wei T, Gooi JH, Quinn JM, Crimeen-Irwin B, Pompolo S, Sims NA, Gillespie MT, Onyia JE, Martin TJ 2008 EphrinB2 regulation by PTH and PTHrP revealed by molecular profiling in differentiating osteoblasts. J Bone Miner Res **23**(8)**:**1170-1181.
32. Turner CH, Burr DB 1993 Basic biomechanical measurements of bone: a tutorial. Bone **14**(4)**:**595-608.
33. Schriefer JL, Robling AG, Warden SJ, Fournier AJ, Mason JJ, Turner CH 2005 A comparison of mechanical properties derived from multiple skeletal sites in mice. Journal of biomechanics **38**(3)**:**467-475.
34. Diez-Perez A, Guerri R, Nogues X, Caceres E, Pena MJ, Mellibovsky L, Randall C, Bridges D, Weaver JC, Proctor A, Brimer D, Koester KJ, Ritchie RO, Hansma PK 2010 Microindentation for in vivo measurement of bone tissue mechanical properties in humans. J Bone Miner Res **25**(8)**:**1877-1885.
35. Sims NA, Dupont S, Krust A, Clement-Lacroix P, Minet D, Resche-Rigon M, Gaillard-Kelly M, Baron R 2002 Deletion of estrogen receptors reveals a regulatory role for estrogen receptors-beta in bone remodeling in females but not in males. Bone **30**(1)**:**18-25.
36. Davey RA, Clarke MV, Sastra S, Skinner JP, Chiang C, Anderson PH, Zajac JD 2012 Decreased body weight in young Osterix-Cre transgenic mice results in delayed cortical bone expansion and accrual. Transgenic research **21**(4)**:**885-893.
37. Roberts AW, Robb L, Rakar S, Hartley L, Cluse L, Nicola NA, Metcalf D, Hilton DJ, Alexander WS 2001 Placental defects and embryonic lethality in mice lacking suppressor of cytokine signaling 3. Proc Natl Acad Sci U S A **98**(16)**:**9324-9329.
38. Xiao Z, Dallas M, Qiu N, Nicolella D, Cao L, Johnson M, Bonewald L, Quarles LD 2011 Conditional deletion of Pkd1 in osteocytes disrupts skeletal mechanosensing in mice. FASEB J **25**(7)**:**2418-2432.
39. Sheng MH, Zhou XD, Bonewald LF, Baylink DJ, Lau KH 2013 Disruption of the insulin-like growth factor-1 gene in osteocytes impairs developmental bone growth in mice. Bone **52**(1)**:**133-144.
40. Cornish J, Callon K, King A, Edgar S, Reid IR 1993 The effect of leukemia inhibitory factor on bone in vivo. Endocrinology **132**(3)**:**1359-1366.
41. Sims NA 2009 gp130 signaling in bone cell biology: multiple roles revealed by analysis of genetically altered mice. Mol Cell Endocrinol **310**(1-2)**:**30-39.
42. Epelboym Y, Gendron RN, Mayer J, Fusco J, Nasser P, Gross G, Ghillani R, Jepsen KJ 2012 The interindividual variation in femoral neck width is associated with the acquisition of predictable sets of morphological and tissue-quality traits and differential bone loss patterns. J Bone Miner Res **27**(7)**:**1501-1510.
43. Mantila Roosa SM, Liu Y, Turner CH 2011 Gene expression patterns in bone following mechanical loading. J Bone Miner Res **26**(1)**:**100-112.

44. Qiu S, Rao DS, Palnitkar S, Parfitt AM 2002 Relationships between osteocyte density and bone formation rate in human cancellous bone. Bone **31**(6)**:**709-711.
45. Bellido T, O'Brien CA, Roberson PK, Manolagas SC 1998 Transcriptional activation of the p21(WAF1,CIP1,SDI1) gene by interleukin-6 type cytokines. A prerequisite for their pro-differentiating and anti-apoptotic effects on human osteoblastic cells. J Biol Chem **273**(33)**:**21137-21144.
46. Gabay C, Emery P, van Vollenhoven R, Dikranian A, Alten R, Pavelka K, Klearman M, Musselman D, Agarwal S, Green J, Kavanaugh A, Investigators AS 2013 Tocilizumab monotherapy versus adalimumab monotherapy for treatment of rheumatoid arthritis (ADACTA): a randomised, double-blind, controlled phase 4 trial. Lancet **381**(9877)**:**1541-1550.
47. Schwache D, Muller-Newen G 2012 Receptor fusion proteins for the inhibition of cytokines. European journal of cell biology **91**(6-7)**:**428-434.
48. Jones SA, Scheller J, Rose-John S 2011 Therapeutic strategies for the clinical blockade of IL-6/gp130 signaling. J Clin Invest **121**(9)**:**3375-3383.
49. Waetzig GH, Rose-John S 2012 Hitting a complex target: an update on interleukin-6 trans-signalling. Expert opinion on therapeutic targets **16**(2)**:**225-236.

Figure legends

Figure 1. Verification of gp130 functional knockdown by Osx1Cre and DMP1Cre. (A) Osterix1Cre GFP-expressing neonatal calvarial cells from *Osx1Cre.gp130*$^{w/w}$ and *Osx1Cre.gp130*$^{f/f}$ mice were freshly isolated and FACS sorted for the GFP positive population. Knockdown of gp130 was assessed by qPCR using primers targeted to the transmembrane domain (exon 15) of gp130 (n=2 *w/w* and n=3 *f/f* litters of pooled pups collected in independent experiments). (B) Femurs collected from 12 week-old *DMP1Cre.gp130*$^{w/w}$ and *DMP1Cre.gp130*$^{f/f}$ male and female mice flushed of bone marrow were assessed for gp130 knockdown by qPCR with exon 15-directed primers (males, n= 8 mice/group, females, n=5 *w/w* and n=8 *f/f* mice/group). (C) Mouse OSM (0.2µg in 25µl) was administered for 5 sequential days over the calvaria of *DMP1Cre.gp130*$^{w/w}$ and *DMP1Cre.gp130*$^{f/f}$ 6 week-old females. Calvaria were collected 10 days following the last injection (gp130 *w/w* mice: n=8 vehicle, n=7 mOSM; gp130 *f/f* mice: n=9 vehicle, n=8 mOSM). For all graphs, columns represent mean/group and error bars indicate standard error mean, where *p<0.05, **p<0.01, ***p<0.001.

Figure 2. Conditional deletion of gp130 throughout the osteoblast lineage reduces trabecular bone in adult male mice. Trabecular bone structure was assessed by microCT (SkyScan) in 12 and 26 week-old male *Osx1Cre.gp130* mice for (A) % bone volume/tissue volume (BV/TV), (B) trabecular thickness (TbTh), (C) trabecular number (TbN), and (D) trabecular spacing (TbSp) in the metaphysis of the distal femur. MicroCT images were produced in ParaView (E) and represent the average value for trabecular bone structures in (A-D) (12 week-old mice: n=8 *w/w*, n=7 *f/f*; 26 week-old mice: n=8 *w/w* and n=8 *f/f*). For all

graphs, single plot points represent mean/group and error bars indicate standard error mean, where **p<0.01, ***p<0.001, ****p<0.0001. See also Figure S1 and Figure S2.

Figure 3. gp130 deletion in osteocytes reduces trabecular bone in adult male mice. Trabecular bone structure of *DMP1Cre.gp130* mice was assessed by microCT (SkyScan) in 12 and 26 week-old male mice for (A) % bone volume/tissue volume (BV/TV), (B) trabecular thickness (TbTh), (C) trabecular number (TbN), and (D) trabecular spacing (TbSp) in the distal femur. MicroCT images were produced in ParaView (E) and represent the average value for trabecular bone structures in (A-D) (12 week-old mice: n=8 *w/w*, n=12 *f/f*; 26 week-old mice: n=8 *w/w* and n=8 *f/f*). For all graphs, single plot points represent mean/group and error bars indicate standard error mean, where *p<0.05, **p<0.01, ***p<0.001, ****p<0.0001. See also Figure S3 and Figure S4.

Figure 4. Conditional deletion of gp130 in osteoblasts and osteocytes lowers bone formation rate and mineralisation in adult male and female mice. 12 week-old male and female mice were evaluated for dynamic markers of bone formation following calcein injection 10 days and 3 days prior to cull. (A) male *DMP1Cre.gp130* mice (n=8 *w/w*, n=5 *w/f*, n=12 *f/f*), (B) male *Osx1Cre.gp130* mice (n=10 *w/w*, n=5 *w/f*, n=6 *f/f*), (C) female *DMP1Cre.gp130* mice (n=5 *w/w*, n=6 *w/f*, n=9 *f/f*) and (D) female *Osx1Cre.gp130* mice (n=8 *w/w*, n=8 *w/f*, n=7 *f/f*) were analysed using Osteomeasure to determine bone formation rate/bone surface (BFR/BS), double-labelled surface (dLS/BS), and mineral apposition rate (MAR) in the trabecular bone of the proximal tibia. For all graphs, columns represent mean/group and error bars indicate standard error mean, where *p<0.05.

Figure 5. Cortical diameter is increased with gp130 deletion. The femoral diaphysis of 12 and 26 week-old male mice was analysed by microCT (SkyScan) for cortical bone structure. Periosteal perimeter (Ps Perim), cross-sectional moment of inertia (CSMI), and marrow area are reported for (A) *DMP1Cre.gp130* (12 week-old mice: n=8 *w/w*, n=12 *f/f*; 26 week-old mice: n=8 *w/w* and n=8 *f/f*) and (C) *Osx1Cre.gp130* (12 week-old mice: n=8 *w/w*, n=8 *f/f*; 26 week-old mice: n=8 *w/w* and n=8 *f/f*) mice. (B) Anterior-posterior and lateral-medial width was measured for each bone by digital callipers at the femoral mid-shaft of 26-week old *DMP1Cre.gp130*$^{w/w}$ (males n=8, females n=5) and *DMP1Cre.gp130*$^{f/f}$ (males n=8, females n=8) mice. (D, E) Periosteal bone formation was quantified by dynamic markers of bone formation in the tibia midshaft using Osteomeasure. Calcein was injected into mice 10 and 3 days prior to cull and trans-axial histological sections from the tibia of (D) *DMP1Cre.gp130* (n=10 *w/w*, n=11 *f/f*) and (E) *Osx1Cre.gp130* mice (n=6 *w/w*, n=10 *f/f*) were assessed for mineralising surface [dLS/BS+1/2(sLS/BS)], double-labelled surface (dLS/BS), single-labelled surface (sLS/BS), bone formation rate (BFR/BS), and mineral apposition rate (PsMAR) on the periosteal surface. For all graphs, the columns or single plot points represent mean/group and error bars indicate standard error mean, where *p<0.05, **p<0.01, ***p<0.001. See also Figure S5.

Figure 6. gp130 deletion in osteocytes reduces material properties of cortical bone in male mice. 26 week-old male (n=8 *w*/w, n=8 *f*/f) or female (n=5 *w/w*, n=7 *f/f*) *DMP1Cre.gp130* mice were subjected to 3-point bending test for assessment of (A) elastic modulus, (B) ultimate stress, (C) yield strength, and (D) work (toughness). (E, F) Load-deformation curves and (G, H) stress-strain curves for male and female mice were also generated from 3-point bending test and represent the average/group. (I) Post-yield stress as assessed by 3-point bending test. (J) Proportion of lamellar *vs* woven bone in 12 week-old

male *DMP1Cre.gp130* mice (n=9 *w/w*, n=8 *f/f*) assessed by polarized light microscopy with representative images. White arrows indicate woven bone, grey arrows indicate lamellar bone. For all graphs, columns represent mean/group and error bars indicate standard error mean, where *p<0.05, **p<0.01. See also Figure S6.

Figure 7. gp130 deletion in osteoblasts increases the proportion of sclerostin-positive osteocytes. Histological sections from 12 week-old male *DMP1Cre.gp130* (n=6 *w/*w, n=7 *f/*f) and *Osx1Cre.gp130* mice (n=12 *w/w*, n=9 *f/f*) were evaluated for (A) total osteocyte number/mm^2 of bone in femoral metaphyseal trabecular and cortical bone. Histological sections were stained for sclerostin by immunohistochemistry and (B) the number of sclerostin-positive osteocytes in trabecular (proximal tibia) and cortical bone (tibia midshaft) were counted manually and normalized to bone area. Paired statistical analyses were used for intra-mouse comparisons. Data is mean+SEM and *p<0.05, **p<0.01, ***p<0.001.

Figure 8. Osteocytic deletion of gp130 reduces OSX, COL1-α1, and OCN gene expression. Femurs collected from 12 week-old *DMP1Cre.gp130*$^{w/w}$ and *DMP1Cre.gp130*$^{f/f}$ mice and flushed of bone marrow were examined for osteoblast and osteocyte markers of gene expression by qPCR (males, n= 8 mice/group, females, n=5 *w/w* and n=8 *f/f* mice/group). Statistical significance between *w/w* and *f/f* bones was reached in (A-C) for osterix, osteocalcin, and collagen type 1-α1 mRNA levels.(D) collagen type 1-α2 was not signficantly altered. (E) Ratio of mRNA levels for collagen type 1-α1: collagen type 1-α2 in flushed femora. (F) No statistical significance between genotypes was detected for runt-related transcription factor 2 (RUNX2), alkaline phosphatase (ALP), receptor activator of NF_kB ligand (RANKL), osteoprotegerin (OPG), matrix extracellular phosphoglycoprotein (MEPE), or sclerostin (SOST) gene expression, all normalised to hydroxymethylbilane

synthase (HMBS). For all graphs, columns represent mean/group and error bars indicate standard error mean, where *p<0.05, **p<0.01.

Figure 9. The physiological role of osteocyte gp130 signalling in bone formation and osteoclastogenesis. (A) Osteoblast/osteocyte gp130 signalling is not required (dashed lines) for normal levels of adipocyte or osteoclast formation, or RANKL expression by osteoblasts. (B) Osteocyte gp130 signalling positively regulates osteoblast differentiation on trabecular bone surfaces (solid lines), and (C) contributes to appropriate collagen production by both trabecular and periosteal osteoblasts (yellow matrix). (D) Periosteal expansion by osteoblasts in response to mechanical forces and osteocyte signals are not dependent on osteocyte gp130 signalling. Solid arrows indicate processes that depend on osteoblast-lineage gp130 expression. Dashed arrows indicate processes that are independent of osteoblast-lineage gp130 expression. OB=osteoblast (dark blue), OC=osteoclast (red), OY=osteocyte (light blue).

Table 1. Primer sequences for semi-quantitative real-time PCR.

All sequences were designed against the mouse genome.

Gene Name	**Direction**	**Sequence**
mB2M	Forward	5'-TTCACCCCCACTGAGACTGAT-3'
	Reverse	5'-GTCTTGGGCTCGGCCATA-3'
mHPRT1	Forward	5'-TGATTAGCGATGATGAACCAG-3'
	Reverse	5'-AGAGGGCCACAATGTGATG-3'
mGP130 (exon 15)	Forward	5'-AGAAGCCATAGTCGTGCCTGTGT-3'
	Reverse	5'-AAAGCAGAACAAGACGCCCAGCA-3'
mRUNX2	Forward	5'-CTCCGCTGTTATGAAAAACC-3'
	Reverse	5'-TGAAACTCTTGCCTCGTCC-3'
mOSX	Forward	5'-ATGGCGTCCTCTCTGCTTG-3'
	Reverse	5'-TGAAAGGTCAGCGTATGGCTT-3'
mOPG	Forward	5'-TGTCCAGATGGGTTCTTCTCA-3'
	Reverse	5'-CGTTGTCATGTGTTGCATTTCC-3'
mMEPE	Forward	5'-AGGCTGTGTCTGTTGGACTG-3'
	Reverse	5'-CTGGTTTCCTTCCCTCCGTA-3'
mHMBS	Forward	5'-TCATGTCCGGTAACGGCG-3'
	Reverse	5'-CACTCGAATCACCCTCATCTTTG-3'

Table 2. Bone cell parameters of DMP1Cre.gp130 and Osx1Cre.gp130 male and female mice at 12 weeks of age.

	DMP1Cre.gp130				***Osx1Cre.gp130***			
	Males		**Females**		**Males**		**Females**	
	w/w	***f/f***	***w/w***	***f/f***	***w/w***	***f/f***	***w/w***	***f/f***
	n=9	***n=11***	***n=6***	***n=8***	***n=15***	***n=14***	***n=15***	***n=8***
ObN/BPm (/mm)	5.74 ± 1.15	4.60 ± 1.21	16.51 ± 2.73	11.51 ± 2.31*	5.21 ± 0.76	6.86 ± 1.15	14.24 ± 0.97	8.12 ± 1.06***
ObS/BS (%)	8.83 ± 1.83	7.35 ± 1.87	24.89 ± 4.53	13.99 ± 1.37*	8.86 ± 1.29	10.85 ± 2.05	25.39 ± 1.98	12.41 ± 1.48***
OS/BS (%)	8.37 ± 1.83	7.08 ± 1.97	24.10 ± 5.35	13.62 ± 1.55*	7.79 ± 1.16	9.83 ± 1.43	18.6 ± 1.65	10.33 ± 1.71**
OV/BV (%)	0.87 ± 0.23	0.91 ± 0.34	3.94 ± 1.02	2.68 ± 0.94	0.87 ± 0.23	1.45 ± 0.29	3.09 ± 0.38	1.57 ± 0.31**
OcN/BPm (/mm)	1.56 ± 0.25	1.83 ± 0.27	1.91 ± 0.23	2.68 ± 0.46	1.36 ± 0.13	1.38 ± 0.17	2.66 ± 0.21	2.01 ± 0.25
OcS/BS (%)	5.98 ± 1.04	7.21 ± 1.35	8.56 ± 1.32	10.47 ± 1.72	6.56 ± 0.81	6.46 ± 0.73	13.88 ± 1.11	11.78 ± 1.77

Osteoblast number/bone perimeter (ObN/BPm), osteoblast surface/bone surface (ObS/BS), osteoid surface (OS/BS), osteoid volume/bone volume (OV/BV), osteoclast number (OcN/BPm), and osteoclast surface (OcS/BS) were manually counted and quantified in the proximal tibia of histological sections from 12 week-old male and female mice. Values/group ± standard error mean and n/group are listed, where *p<0.05, **p<0.01, ***p<0.001.

Table 3. Ultimate properties of *DMP1Cre.gp130* 26 week-old mice.

	> 01(		/(- 01(	
	! "!	#'#	! "!	#'#
$%&## ( ))*+, "- - .	! ! "#$%&%$# (	! ! ' #(%&%)#*+	! , +#) %&%#, !	! ! $#, %&%! #-!
/0&23(*/435(*+, .	! ' #- %&%#) !	! ' # ! %&%#' "	(*#, +%&%#("	( ) # *%&%#(,
6(#43- 0%&4' *0%& /0&23(*+- - .	-#! $%&%# !	-#! $%&%# !	-#(! %&%# !	-#(, %&%# (
7' (389*: ;)43; (<* 0%&/0&23(*+=	-# - ! %&%# - - (	-# - ! %&%# - - ,	-# - (%&%# - !	-# - (%&%# - !

Femora from 26 week-old male (n=8 *w/w*, n=8 *f/f*) and female (n=5 *w/w*, n=7 *f/f*) *DMP1Cre.gp130* mice were subjected to 3-point bending and evaluated for stiffness and ultimate properties (to failure point).

A

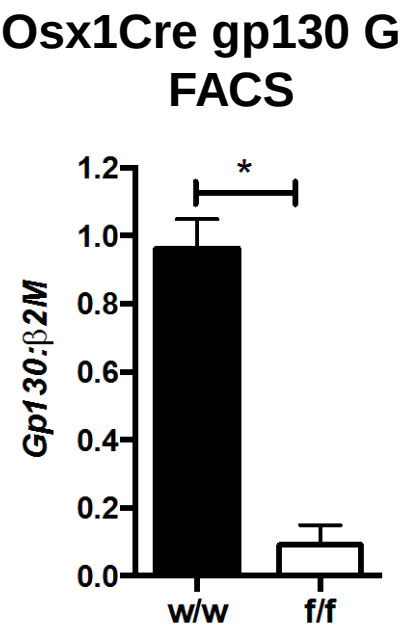
Osx1Cre gp130 GFP FACS
Gp130:β2M
1.2
1.0
0.8
0.6
0.4
0.2
0.0
*
w/w
f/f

B

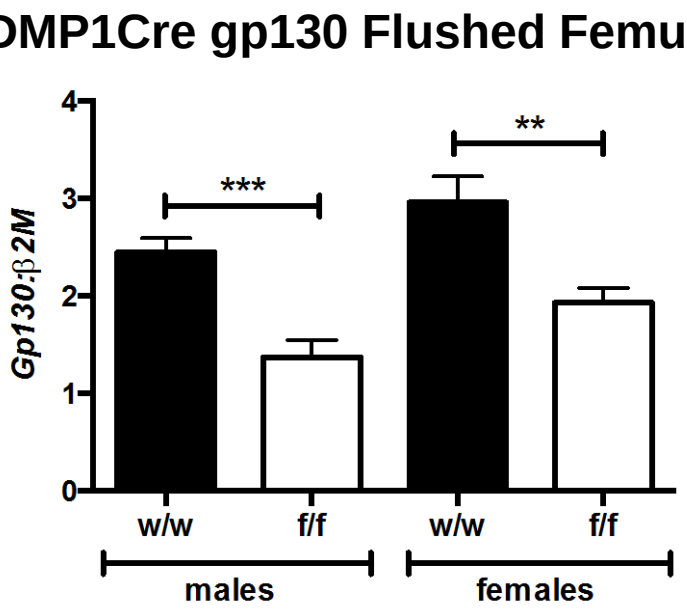
DMP1Cre gp130 Flushed Femurs
Gp130:β2M
4
3
2
1
0
***
**
w/w
f/f
w/w
f/f
males
females

C

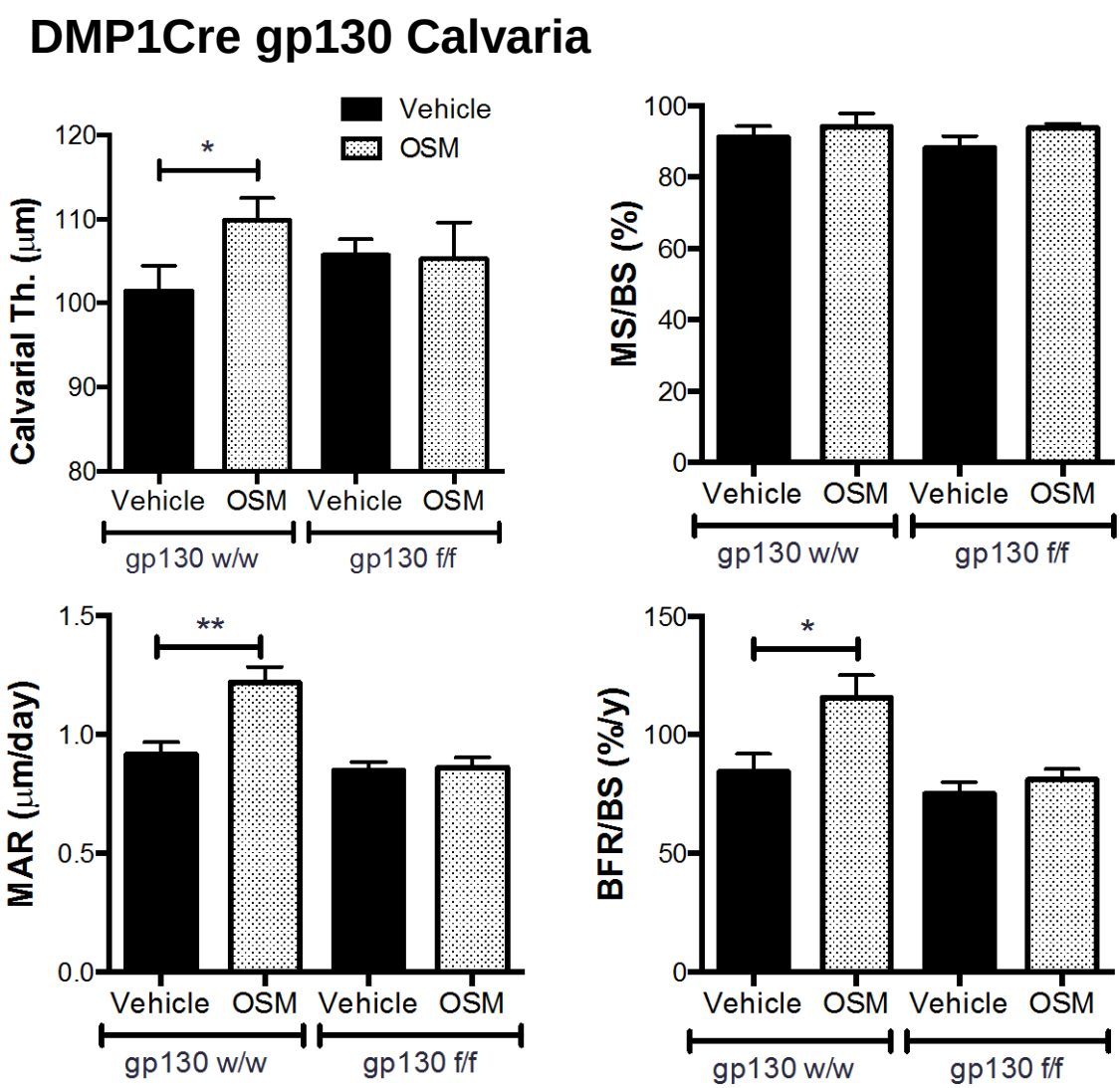
DMP1Cre gp130 Calvaria
Vehicle
OSM
Calvarial Th. (μm)
120
110
100
90
80
*
Vehicle
OSM
Vehicle
OSM
gp130 w/w
gp130 f/f
MS/BS (%)
100
80
60
40
20
0
Vehicle
OSM
Vehicle
OSM
gp130 w/w
gp130 f/f
MAR (μm/day)
1.5
1.0
0.5
0.0
**
Vehicle
OSM
Vehicle
OSM
gp130 w/w
gp130 f/f
BFR/BS (%/y)
150
100
50
0
*
Vehicle
OSM
Vehicle
OSM
gp130 w/w
gp130 f/f

Osx1Cre gp130

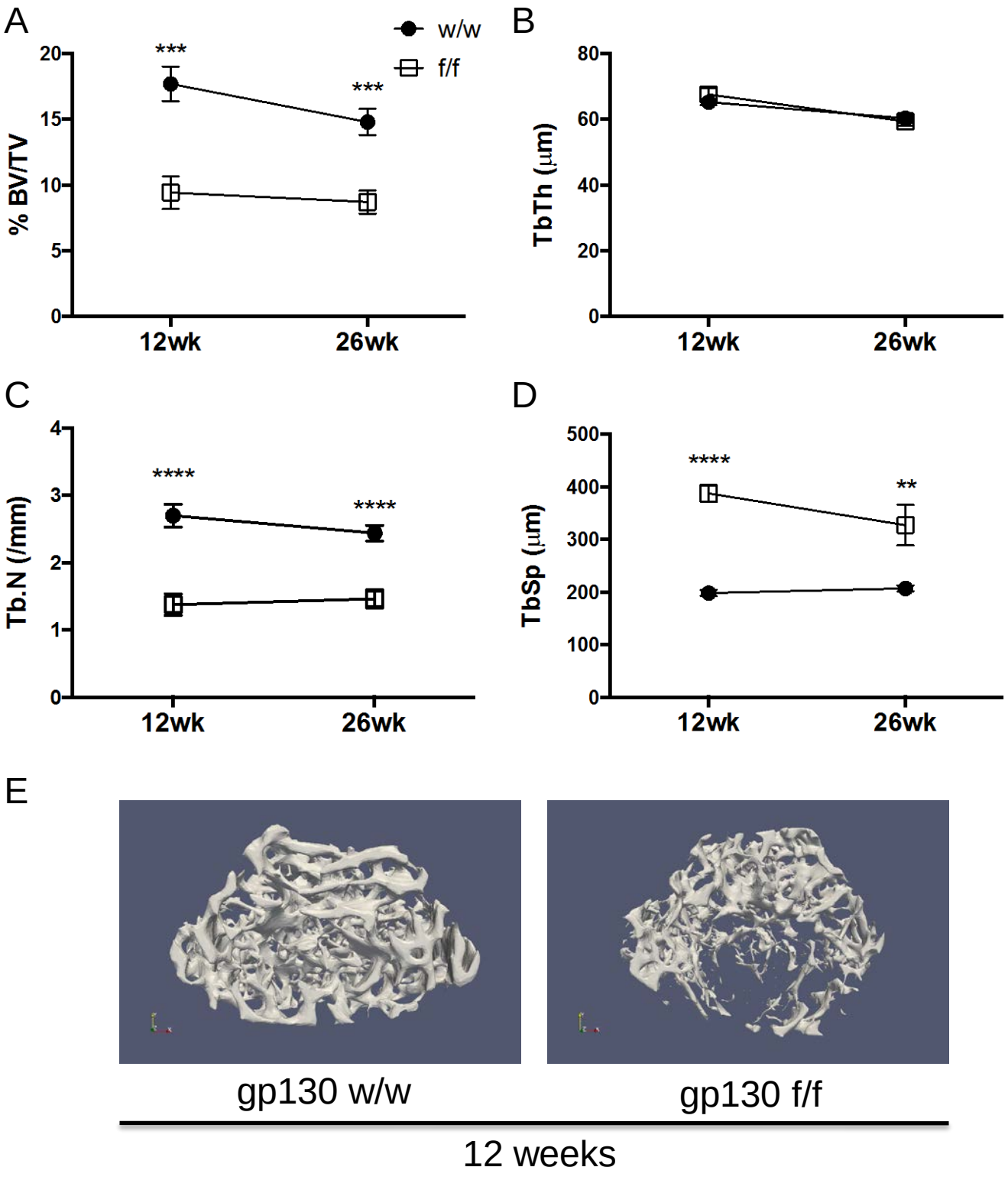

DMP1Cre gp130

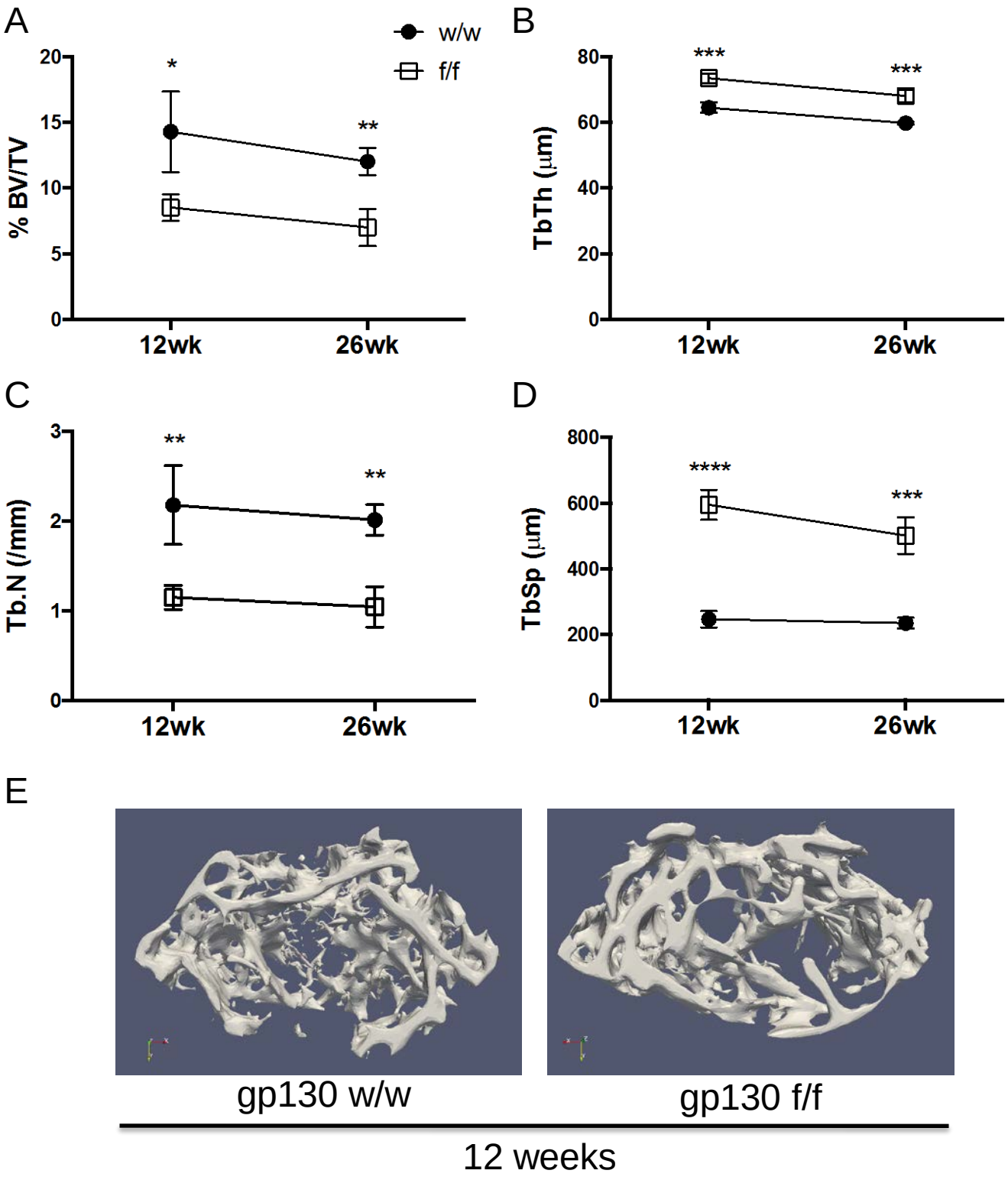

Figure 4

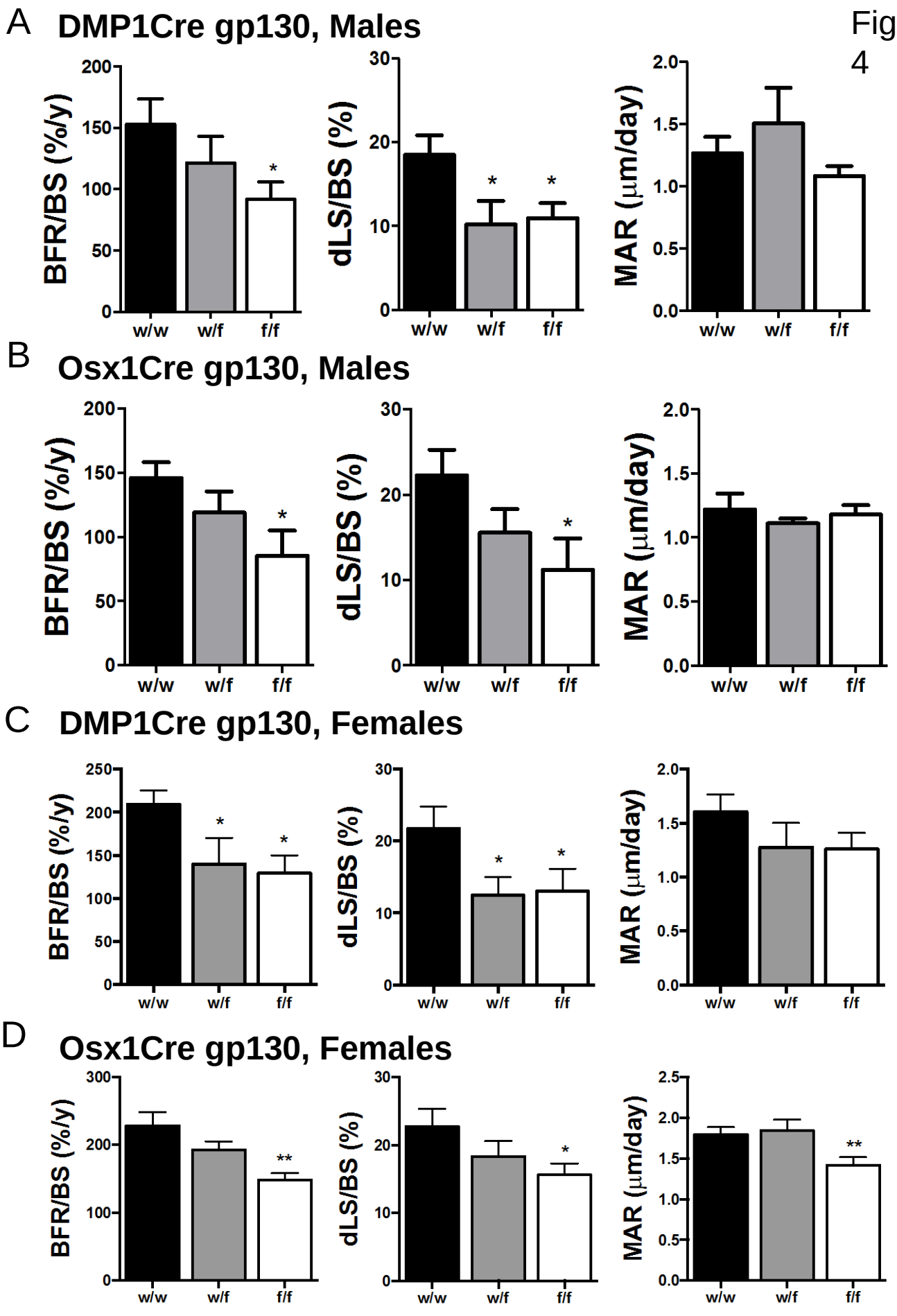
A
DMP1Cre gp130, Males
BFR/BS (%/y)
dLS/BS (%)
MAR (μm/day)
w/w
w/f
f/f
B
Osx1Cre gp130, Males
C
DMP1Cre gp130, Females
D
Osx1Cre gp130, Females

A

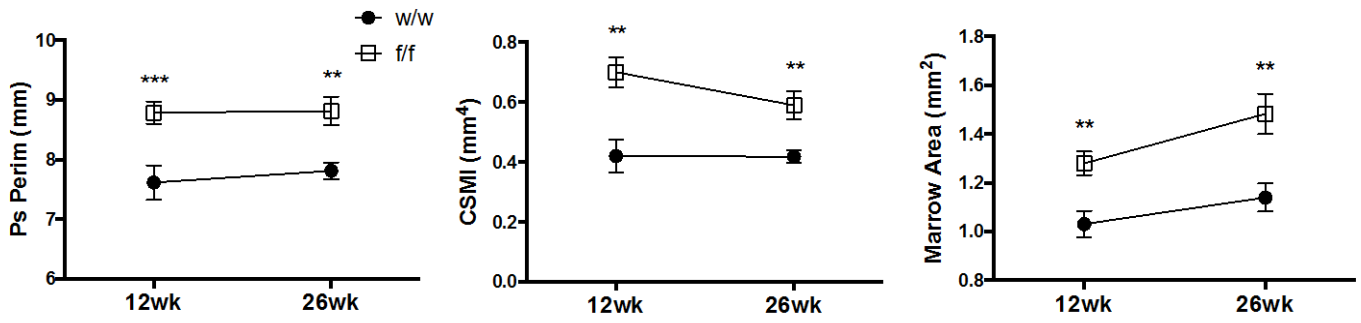
DMP1Cre gp130
w/w
f/f
Ps Perim (mm)
CSMI (mm4)
Marrow Area (mm2)
12wk
26wk

B

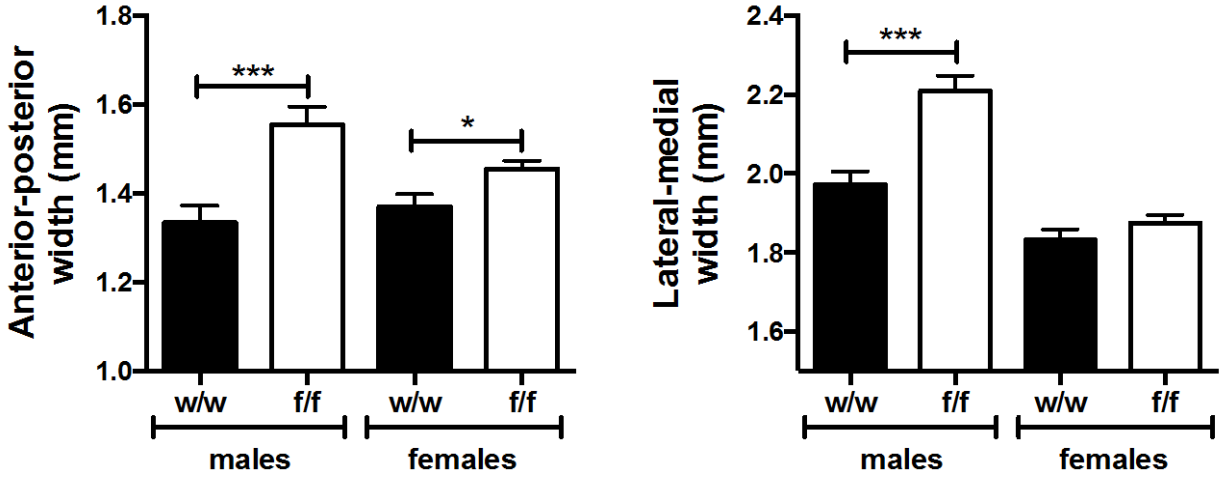
Anterior-posterior width (mm)
Lateral-medial width (mm)
w/w
f/f
males
females

C

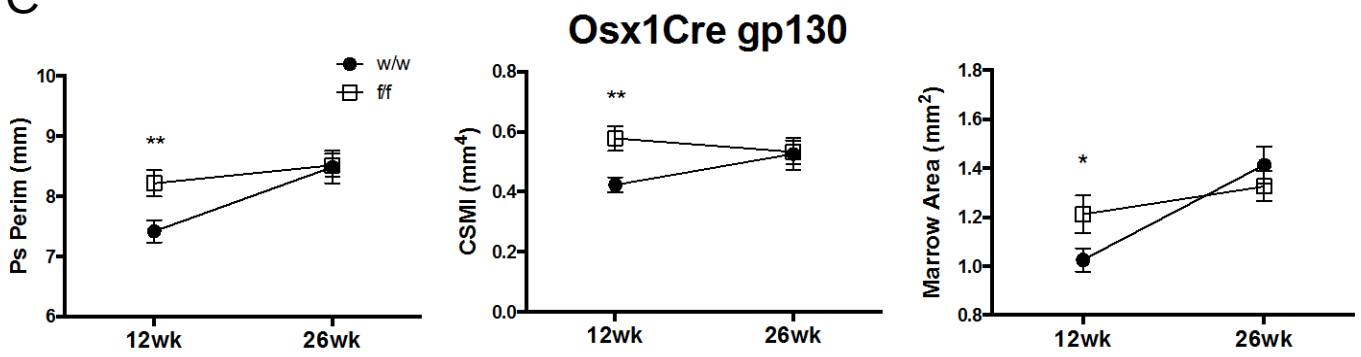
Osx1Cre gp130
w/w
f/f
Ps Perim (mm)
CSMI (mm4)
Marrow Area (mm2)
12wk
26wk

D

DMP1Cre gp130

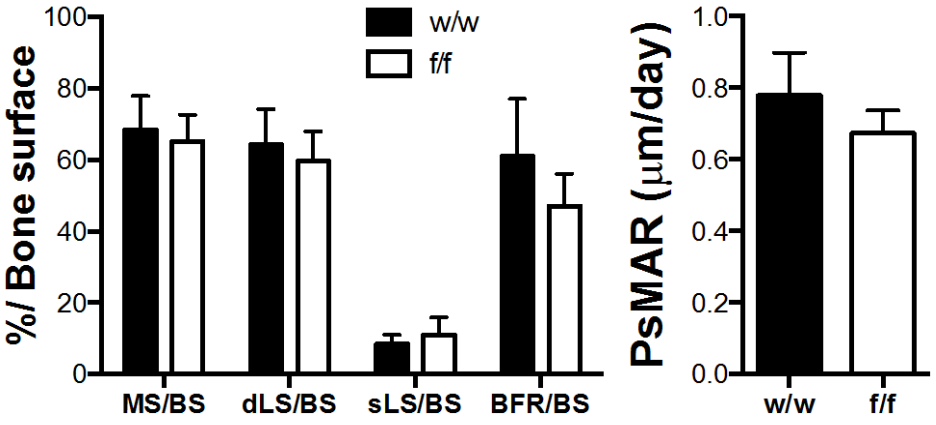

E

Osx1Cre gp130

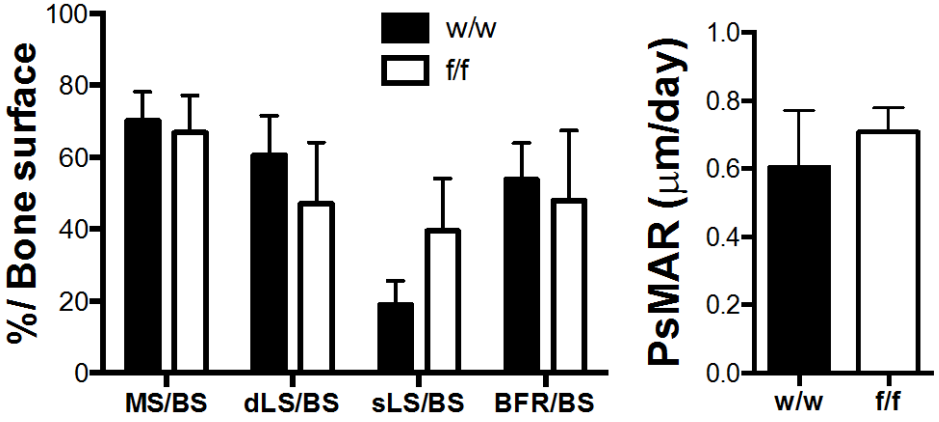

Material Properties

Figure 6

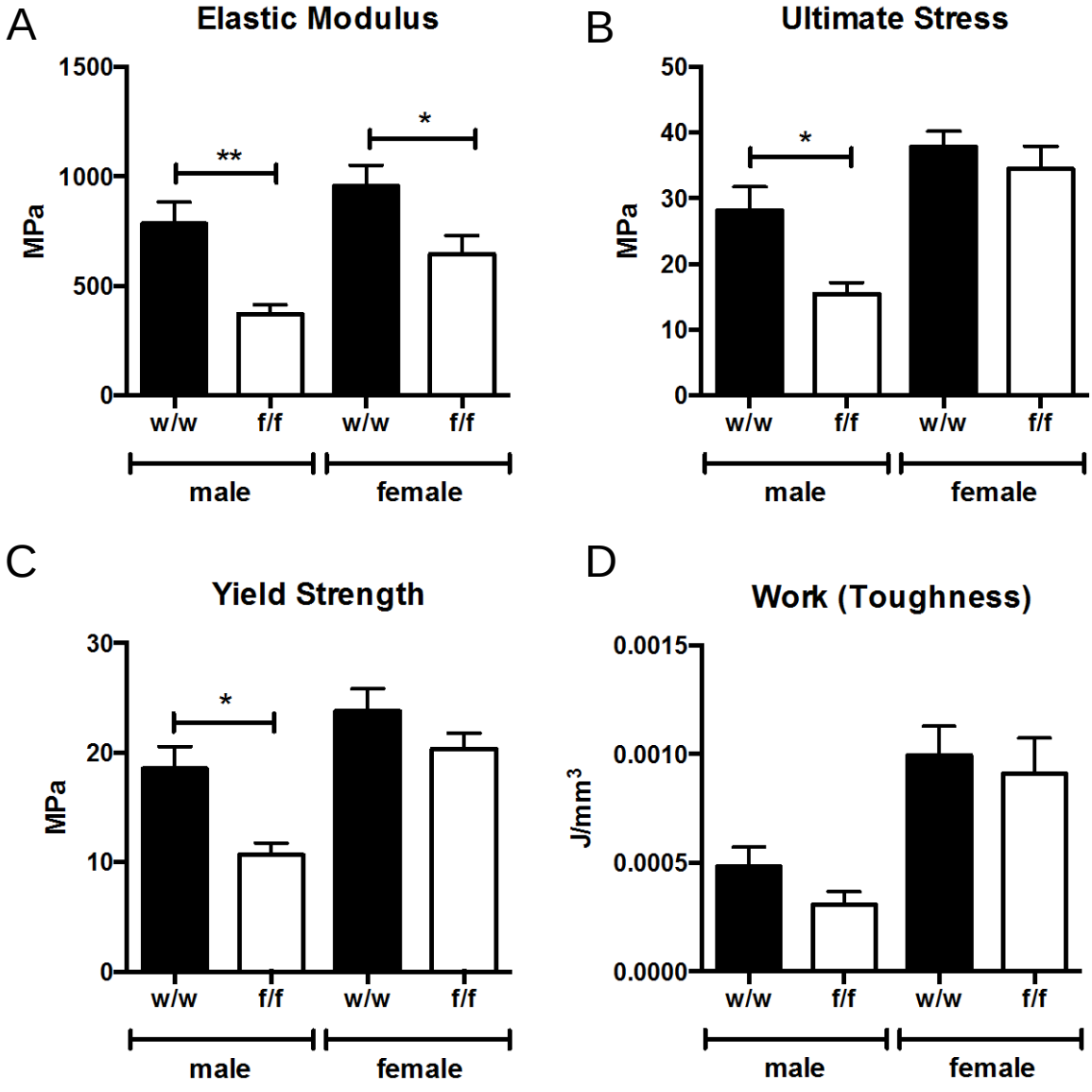

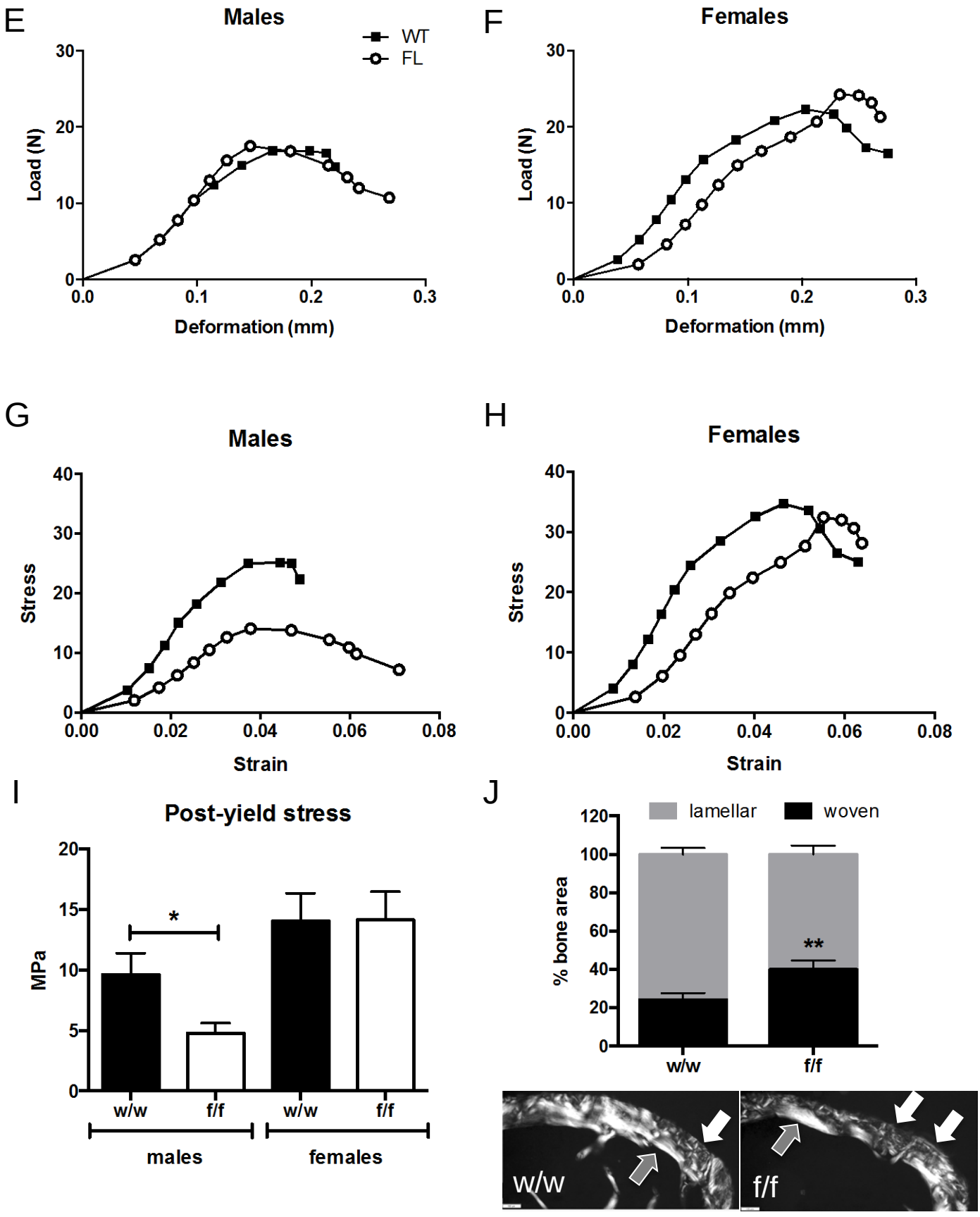
E
Males
WT
FL
Load (N)
Deformation (mm)
F
Females
Load (N)
Deformation (mm)
G
Males
Stress
Strain
H
Females
Stress
Strain
I
Post-yield stress
MPa
*
w/w
f/f
w/w
f/f
males
females
J
lamellar
woven
% bone area
**
w/w
f/f
w/w
f/f

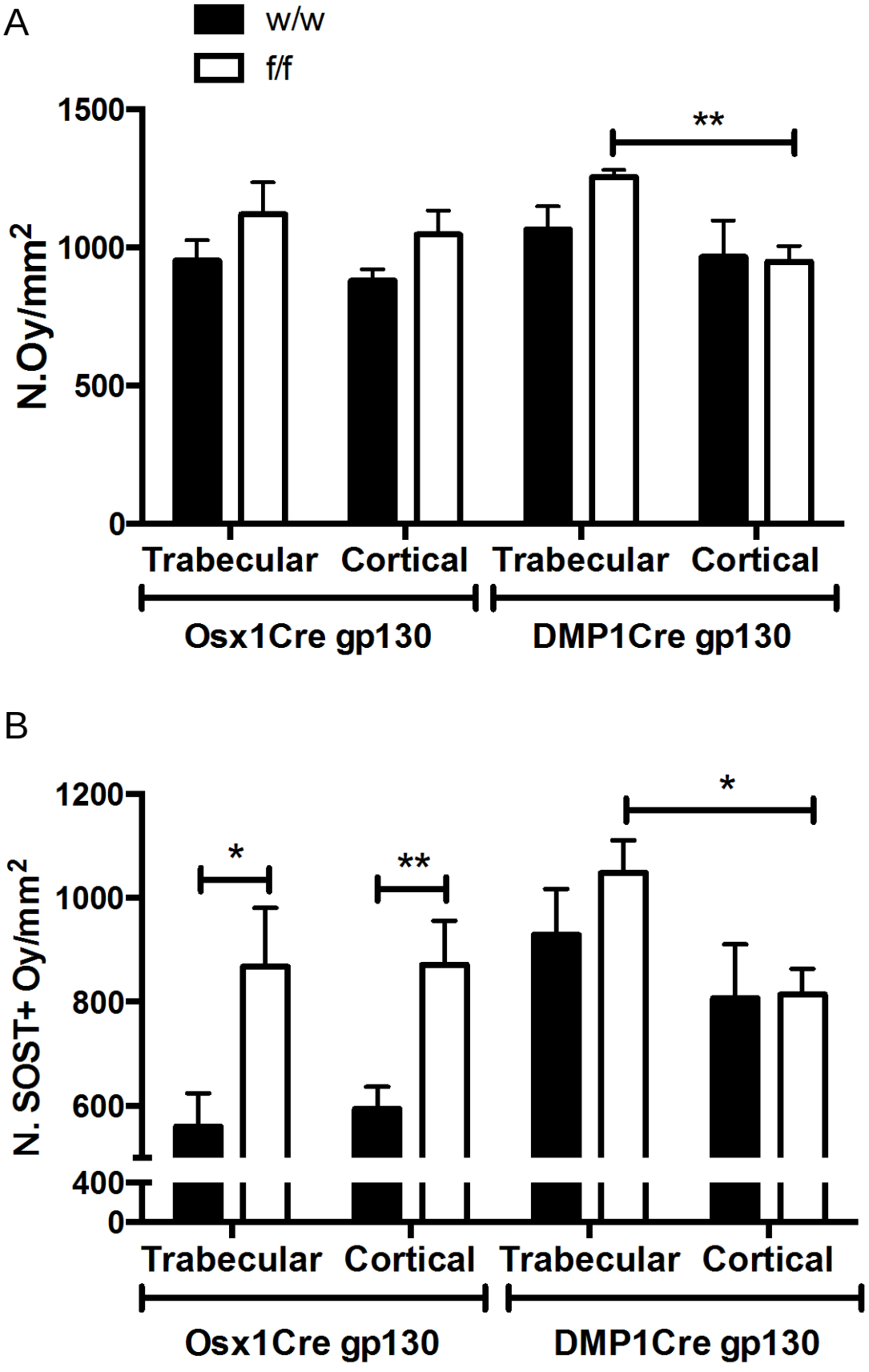
A
w/w
f/f
1500
1000
500
0
N.Oy/mm2
**
Trabecular
Cortical
Trabecular
Cortical
Osx1Cre gp130
DMP1Cre gp130
B
1200
1000
800
600
400
0
N. SOST+ Oy/mm2
*
**
*
Trabecular
Cortical
Trabecular
Cortical
Osx1Cre gp130
DMP1Cre gp130

Figure 8

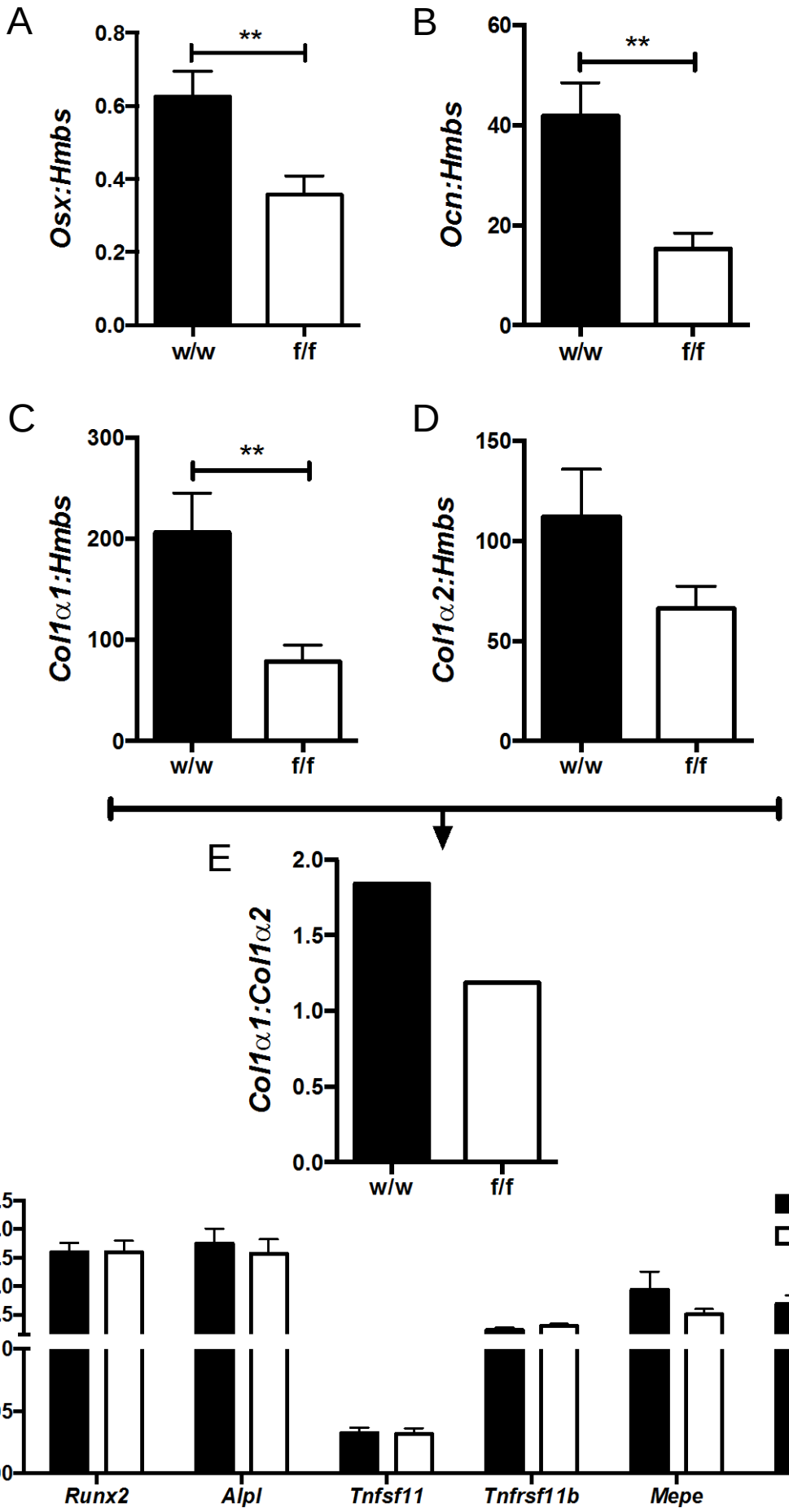
A
Osx:Hmbs
0.8
0.6
0.4
0.2
0.0
**
w/w
f/f
B
Ocn:Hmbs
60
40
20
0
**
w/w
f/f
C
Col1α1:Hmbs
300
200
100
0
**
w/w
f/f
D
Col1α2:Hmbs
150
100
50
0
w/w
f/f
E
Col1α1:Col1α2
2.0
1.5
1.0
0.5
0.0
w/w
f/f
F
mRNA:Hmbs
2.5
2.0
1.5
1.0
0.5
0.10
0.05
0.00
w/w
f/f
Runx2
Alpl
Tnfsf11
Tnfrsf11b
Mepe
Sost

Figure 9

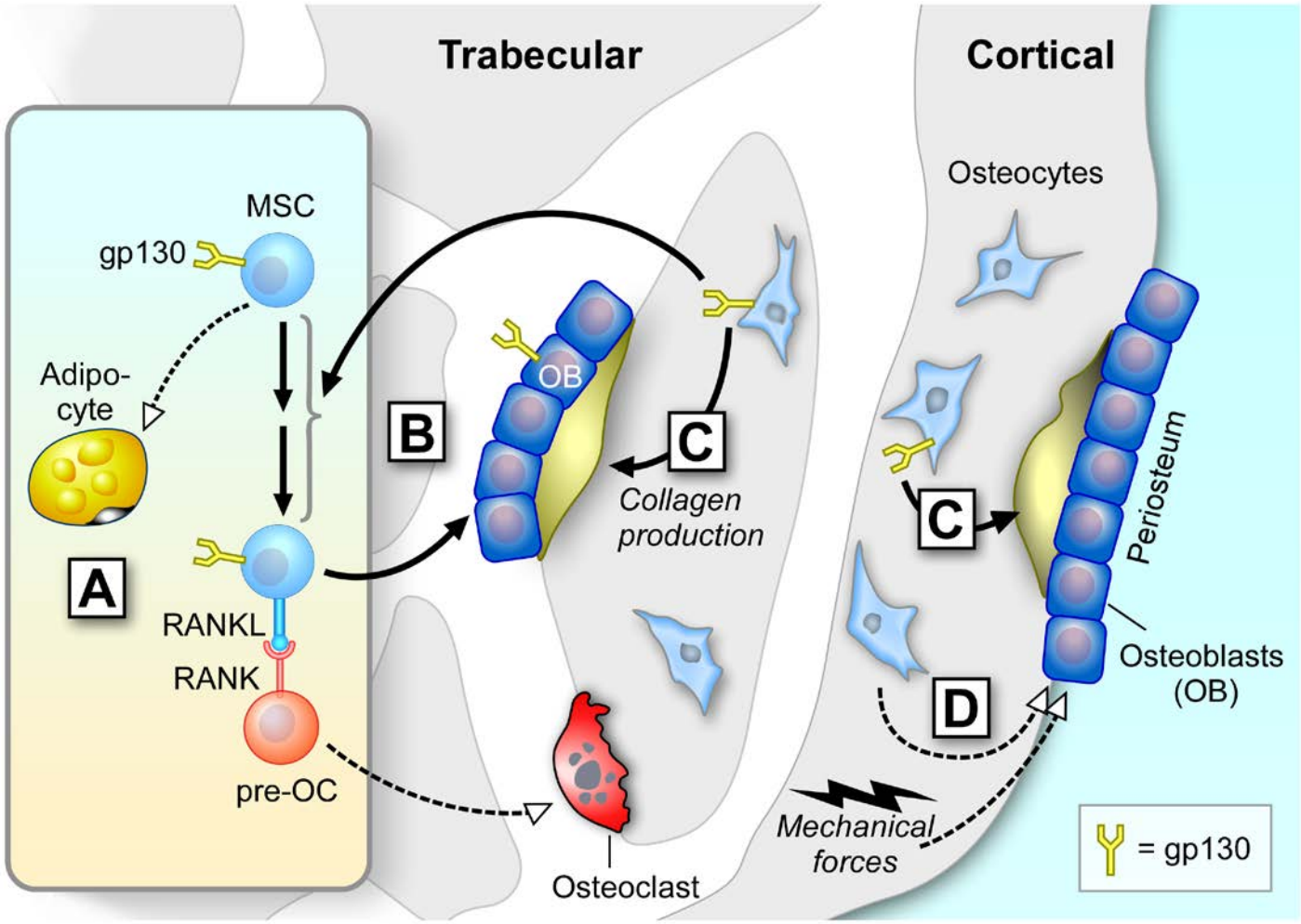
Trabecular
Cortical
MSC
gp130
Adipo-
cyte
A
RANKL
RANK
pre-OC
B
OB
C
Collagen
production
Osteocytes
C
Periosteum
Osteoblasts
(OB)
D
Mechanical
forces
Osteoclast
= gp130